

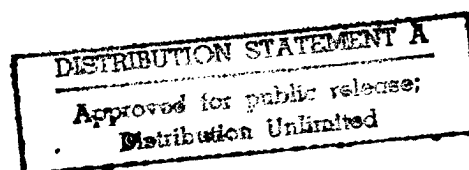
224072

JPRS-JST-88-011

11 JULY 1988



JPRS Report



Science & Technology

Japan

MOLECULAR ULTRATHIN FILM
CONTROL AND DESIGN

19980612 045

REPRODUCED BY
U.S. DEPARTMENT OF COMMERCE
National Technical Information Service
SPRINGFIELD, VA. 22161

DTIC QUALITY INSPECTED 6

10
87
A05

JPRS-JST-88-011

11 JULY 1988

SCIENCE & TECHNOLOGY

JAPAN

MOLECULAR ULTRATHIN FILM CONTROL AND DESIGN

43063801 Wako-shi BUNSHISEI CHOHA KUMAKU in Japanese Jan 88

CONTENTS

ELECTRICAL PROPERTIES OF HYDROPHILIC/HYDROPHOBIC LB FILMS.....	1
ELECTRICAL PROPERTIES OF HYDROPHOBIC POLYMER LB FILMS.....	17
SEM OBSERVATION OF BIOLOGICAL POLYMER LB FILMS.....	29
OPTICAL RECORDING PROPERTIES OF NAPHTHOPHTHALOCYANINE FILM.....	37
PREPARATION OF POLYETHYLENE THIN FILM USING ICB METHOD.....	54
PREPARATION OF PHthalOCYANINE FILM BY OMB METHOD.....	67
ULTRATHIN MONOCRYSTALS USING VAN DER WAALS EPITAXY.....	75

Electrical Properties of Hydrophilic/Hydrophobic LB Films

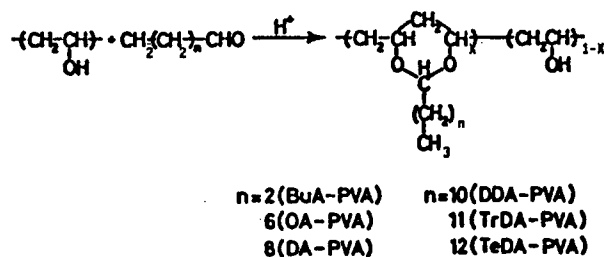
43063801a Wako-shi BUNSHISEI CHOHA KUMAKU in Japanese Jan 88 pp 1-12

[Article by Masayoshi Watanabe and Naoya Ogata, Faculty of Science, Sophia University]

[Text] 1. Introduction

To a large extent the properties of a polymer material are governed by its higher structure as well as by the chemical structure of its constituent molecules. Therefore, to control these properties it is necessary to develop adequate methods for regulating the aggregate state of the polymers. The Langmuir-Blodgett (LB) method has been drawing attention as a means of obtaining films whose thickness and molecular orientation can be controlled at the molecular level, and it has been applied successfully to the preparation of a number of amphipathic compounds. The purpose of the work presented herein was to develop a technique for obtaining films with controlled aggregate states through application of the LB method to amphipathic polymers and to determine their structures and properties. Using a variety of acetalized polyvinyl alcohols, we focused on the question of whether or not these polymers are capable of forming polymeric single-molecule films, evaluated the structure of LB films accumulated on solid substrates and the coagulation state of the secondary polymer chains constituting LB films, and determined the relationship between the coagulation state and electrical properties. The purpose of this article is to present a summary of our findings.

2. Formation of LB Films and Their Structures¹⁻⁴



An acetalized polyvinyl alcohol was obtained by acetalizing commercially available atactic polyvinyl alcohol (PVA) (isotactic diad = 53 percent) using a variety of aldehydes under hydrochloric acid catalysis (see the above formula). The principal polymer employed was PVA having a degree of polymerization of 2000 and an X value of 0.7 to 0.8. Table 1 shows the conditions employed for polymerization and the properties of the resulting polymers. The LB film was built by expanding (using a trough made by the Lauda Corp.) a benzene solution (0.01 wt percent) on purified water (10-11°C). The surface pressure-area curve (F-A curve) was measured (0.5-2.5 cm/min). In addition, the polymer was allowed to build up on a variety of substrates by using the LB method. The rate of accumulation obtained was 0.5-2.5 cm/min.

Table 1. Reaction Conditions and Characterization of Poly(vinyl alkylals)

abbreviation	DP of PVA	reaction conditions ^a					x ^b	T _g ^c , °C	T _d ^d , °C
		aldehyde, g	solvent(vol/vol)	amount of solvent, mL	temp, °C	time, h			
BuA-PVA	2000	7.0	ethanol/water(7/1)	16	40	15	0.72	60	320
OA-PVA	2000	8.0	chloroform	20	40	15	0.75	25	340
	300	8.0	chloroform	20	40	15	0.75	22	340
	1400	8.0	chloroform	20	40	15	0.79	24	330
	2600	8.0	chloroform	20	40	15	0.79	28	330
	2000	8.0	chloroform	20	35	15	0.70	32	330
	2000	5.0	1,4-dioxane/water(3/1)	200	60	20	0.54	50	360
	2000	1.5	1,4-dioxane/water(9/5)	140	60	20	0.40	58	360
	2000	1.0	1,4-dioxane/water(3/2)	100	60	20	0.34	63	350
DA-PVA	2000	8.0	chloroform	20	40	15	0.74	22	340
DDA-PVA	2000	8.0	chloroform	20	40	15	0.73	13	350
TrDA-PVA	2000	10.0	chloroform	20	40	20	0.78	3	340
TeDA-PVA	2000	10.0	chloroform	20	40	20	0.76	5	350

^a For the reaction of PVA(1.0 g). ^b Mole fraction of alkylalized unit determined by elemental analysis. ^c Glass transition temperature determined by differential scanning calorimetry.

^d Starting temperature of weight loss in air determined by thermogravimetry.

Figure 1 shows the F-A curve of the acetalized PVA (X = 0.72 - 0.78). From the illustration it can clearly be seen that with reductions in surface area there is a rapid rise in surface pressure, resulting in the formation of a coagulated film. A further reduction in surface area beyond the inflection point collapses the film. The plateau region beyond the inflection point corresponds with the conformational change, reflecting a balance between the hydrophilicity and hydrophobicity of polymer chains. The limiting area was approximately 30 Å², independent of the side chain length or the molecular weight of the starting PVA (Table 2), which would correspond to an acetal component area of 35 Å², assuming a PVA unit area of 12 Å², in good agreement with the molecular model to be described later. Further, determination of the acetal component area from the limiting area (Table 2) of the F-A curves of samples whose acetalization rates have been changed by using OA-PVA indicates that samples having an X value of 0.40 or less have an acetal area substantially less than 35 Å². Conversely, the determination of the PVA unit area assuming an acetal component area of 35 Å², indicates 6 Å², suggesting that in a strict sense the film is not a

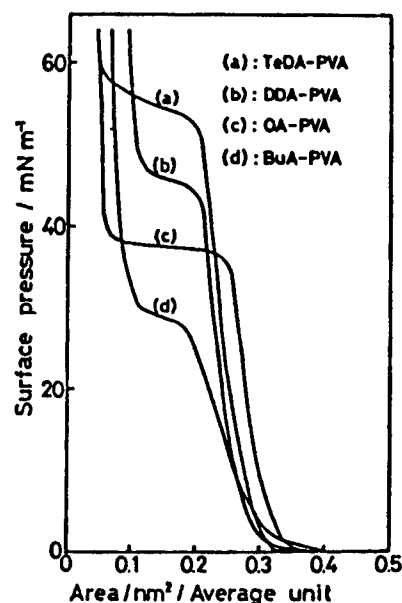


Figure 1. F-A Isotherms of Poly(vinyl alkylal)s

Table 2. Results of Limiting Area of Poly(vinyl alkylals) Found in F-A Isotherms

abbreviation	DP of PVA	x^a	limiting area	
			m ² /mg	nm ² /average repeat unit
BuA-PVA	2000	0.72	1.58	0.30
OA-PVA	2000	0.75	1.16	0.31
	300	0.75	1.16	0.31
	1400	0.79	1.15	0.32
	2600	0.79	1.15	0.32
	2000	0.70	1.13	0.29
	2000	0.54	1.19	0.25
	2000	0.40	1.01	0.18
	2000	0.34	1.03	0.17
DA-PVA	2000	0.74	1.00	0.30
DDA-PVA	2000	0.73	0.86	0.28
TrDA-PVA	2000	0.78	0.82	0.30
TeDA-PVA	2000	0.76	0.76	0.29

^a Mole fraction of alkylalized unit.

monomolecular film, but rather it has a structure wherein the PVA unit lies below the water surface in a loop-like shape. These results indicate that the molecular size of a coagulated film is governed by its major chain structure, rather than by its side chain length or molecular weight. Also, in acetalized PVA having an X value of 0.7 to 0.8, it is thought that the major chains of the polymer are densely packed, forming a monomolecular film.

Use of the LB method on coagulated film samples having X values of 0.7 to 0.8 permitted a buildup of Y films with a buildup ratio of 1.0 on various substrates. The optimal buildup pressures were 25, 30, 32, and 36 mN/m, respectively, on BuA-PVA, OA-PVA, DDA-PVA, and TeDA-PVA samples. The film thicknesses of built-up films and the numbers of layers showed desirable proportional relations (Figure 2). When the results of volume measurements, to be described later, were taken into consideration, it was clear that each layer contained 1 to 100 built-up films of the same film thickness. It was also determined that the longer the methylene chain, the greater was the film thickness per layer. In BuA-PVA, OA-PVA, DDA-PVA, and TeDA-PVA samples, the film thicknesses per layer, respectively, were 8.5, 10.5, 14.0, and 16.5 Å. An evaluation of the effect of molecular weight on film thickness in the OA-PVA sample indicated a film thickness-buildup relationship similar to the results shown in Figure 2.

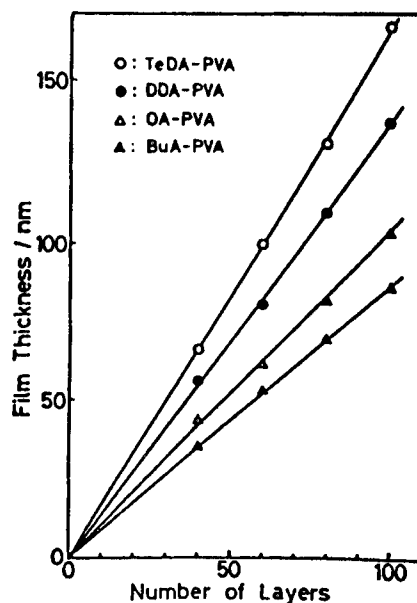


Figure 2. Thickness of Built-Up Films of Poly(vinyl alkylal)s as a Function of Number of Layers

On an aluminum substrate, the wettability of built-up films changed periodically, depending on whether the number of built-up films was odd or even (Figure 3). In a sample containing six layers or more, the wettability of a spin-coating film was the midpoint between the wettability of an odd number of films and the wettability of an even number of films. On the aluminum substrate, films tended to build up as soon as the substrate was lifted. The periodic variation in wettability contrasted with the fact that in the barium salt built-up film of stearic acid the wettability did not depend on odd/even numbers and did not undergo a $\cos\theta - 0.1$ change, indicating the stability of the molecular aggregate state in polymer built-up films.

The above results are consistent with the fact that the expanded acetalized PVA extended its main chains on the water surface, formed a monomolecular film facing both the gaseous and aqueous phases, wherein the side chains

were oriented perpendicular to the water surface, and that this structure was built up on a solid substrate without being destroyed. Thus, the results would seem to suggest that the LB method can be applied to the formation of a hydrophilic/hydrophobic polymer, affording a means of controlling the higher structures of ultrathin films.

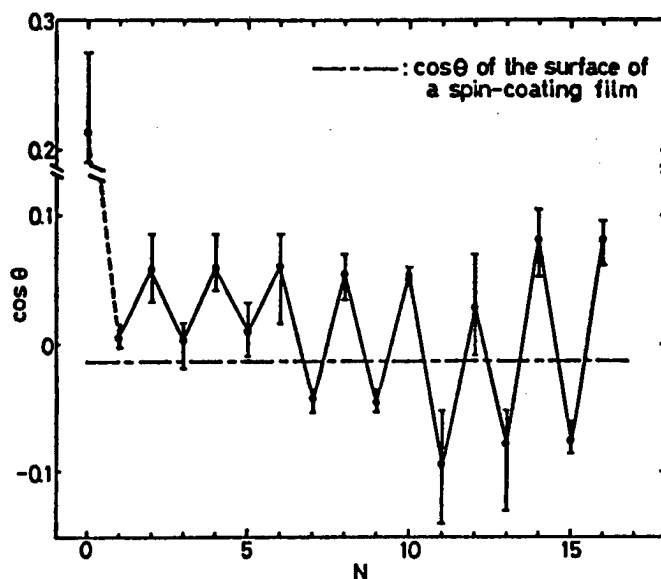


Figure 3. Wettability of Surfaces of Built-Up Films of OA-PVA as a Function of Number of Layers

3. Coagulation State of Secondary Polymer Chains^{4,5}

The configuration¹ of acetalized PVA, made from atactic PVA, was studied by H-NMR spectra. Figure 4(a) and (b) shows, respectively, the NMR spectra of methyl proton positions 4 and 6 of an acetal model compound synthesized from a meso-racemic mixture of 2,4-pentanediol and an acetal model compound made from a racemic mixture and butylaldehyde. Previous investigation⁶ concerning the H-NMR spectra of the structure of 2,4,6-trimethyl-1,3-dioxane¹ showed that there are no possibilities of: 1) axial replacement of the methyl group at position 2; 2) a boat structure of 1,3-dioxane ring; or 3) exchange reaction between the two chair structures at -77 to 150°C. Since the replacement group at position 2 of this model compound is even bulkier, the above possibilities are even less. Therefore, the stereostructure of the model compound would seem to be restricted to possibilities I and II in Figure 4. In contrast to the fact that the methyl proton in compound I, obtained from the meso form, is equivalent, the methyl proton in compound II obtained from the racemic mixture is nonequivalent, and is assigned as shown in the illustration. Figure 5 shows the NMR spectra of OA-PVA ($X = 0.70$). In structure I, the main chain generated from an isotactic diad of PVA is a cis-replaced acetal ring, whereas in structure II, the main chain generated from a syndiotactic diad

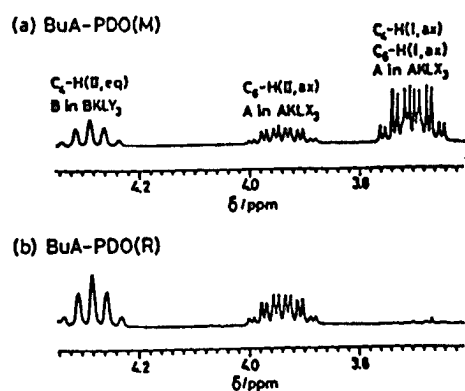
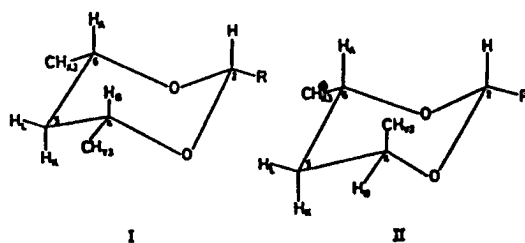


Figure 4. Stereostructures and ^1H -NMR Spectra of 4,6-Dimethyl-2-Propyl-1,3-Dioxane
 (a) From mixtures of meso and racemic forms of 2,4-pentanediol;
 (b) From racemic form of 2,4-pentanediol

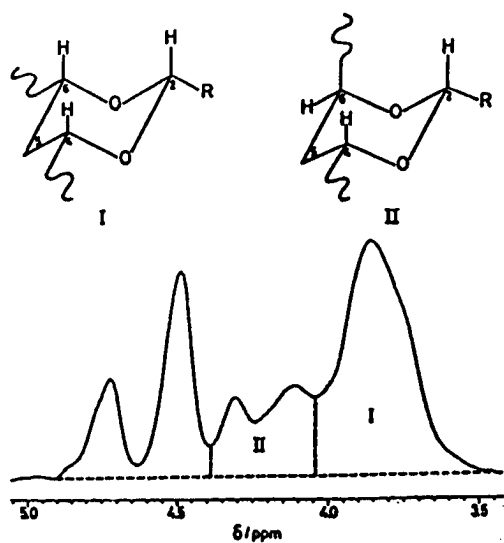


Figure 5. Stereostructures and ^1H -NMR Spectrum of OA-PVA ($X = 0.70$)

is a trans-replaced acetal ring. From these studies on model compounds, the methyl protons at positions 4 and 6 were assigned as shown in the illustration.

Thus, it is apparent that the structure of OA-PVA can be expressed by the above formula. In view of the fact that the starting material PVA contained 53 percent isotactic diad, it would be reasonable to assume that most of the isotactic diad was acetalized, in agreement with the experimental observation⁷ that 1,3-dioxane ring with cis-4,6 replacement formed substantially faster than the trans-4,6 replacement version did.

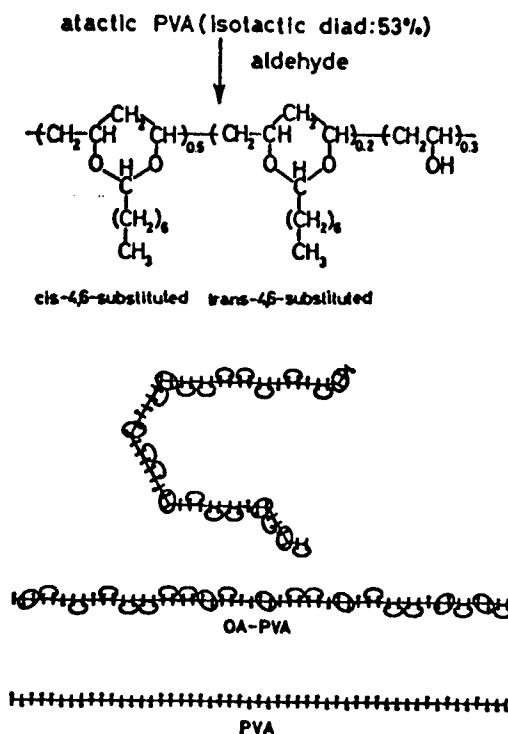


Figure 6. Schematic Diagram for Structures of Atactic PVA and OA-PVA

Based on the above results, we investigated the structure of the monomolecular film of acetalized PVA. Figure 6 shows models of atactic PVA and its acetalized compound. Assuming that the main chains spread either on the water surface or the substrate surface and that the side chains are oriented perpendicular to the surface and stick out from one side only, the degree of conformational freedom of the main chains will be exceedingly low. A reasonable structure for the acetalized part formed from an isotactic diad and the part in which the PVA units are continuous would be one in which the main chains are stretched and have a trans-zigzag structure in the layer perpendicular to the substrate. At the junction of the acetal part formed from an isotactic diad and that formed from a syndiotactic diad, the main chains bend. Consequently, as a whole the main chains are thought to have a two-dimensionally bent conformation, as shown

at the top of Figure 6. Figure 7 [not reproduced] shows a CPK model of such a monomolecular film structure in reference to BuA-PVA as an example. This structure can account for the film thickness per layer in an LB film, the side chain-length dependency of this thickness, and changes in wettability.

The characteristics of the F-A curve suggest that the LB film is a buildup of monomolecular films consisting of highly coagulated two-dimensionally bent chains.

4. Electrical Properties of LB Film on an Aluminum Substrate^{5,8}

Frozen free volume is thought to exist in ordinary three-dimensional amorphous polymers even at T_g or less. The study of the coagulation state of two-dimensional polymer chains, such as the present polymer systems, is of considerable interest. To investigate the degree of uniformity of these LB films, it is useful to consider their electrical properties; also the question of to what extent the orientation structure is reflected in electrical properties is of considerable interest.

As acetalized PVAs we chose BuA-PVA ($X = 0.72$) and OA-PVA ($X = 0.70$), and built up a monofilm on a glass substrate on which aluminum had been vapor-deposited (surface resistance < 15 ohms). The upper Al electrode ($A = 0, 15 \pm 0.02$ cm²) was vapor-deposited through a metal mask (5×10^{-5} torr, for 7 minutes), forming a sandwiched cell as shown in Figure 8. After the upper electrode was vapor-deposited and before being subjected to electrical property measurements, the LB film was dried for at least 5 days using a desiccator containing silica-gel. Contact between the electrode and gold wire was provided by In. Capacitance was measured by using an impedance analyzer (1 kHz, oscillation level 5-10 mV) and DC conductivity was determined from the current response relative to triangular pulse voltage (V_{max}) = +50 mV) at an ultralow frequency of 5×10^{-4} Hz or less. All measurements were conducted in a highly pure nitrogen atmosphere.

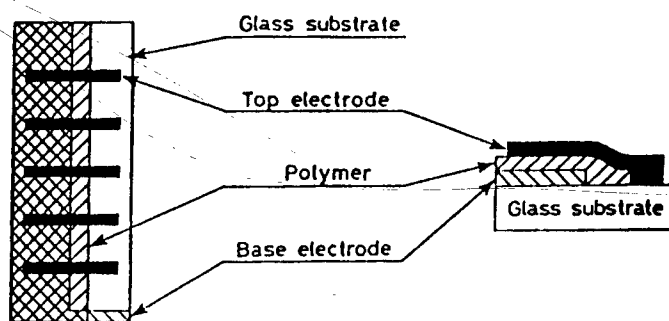


Figure 8. Electrode Arrangement for Electrical Measurements

The capacitance of OA-PVA and BuA-PVA showed virtually no temperature dependency (145 - 293 K), regardless of the number of built-up films involved.¹⁻³⁰ Figure 9 shows the relationship between reciprocal capacitance and the number of built-up films found. In either OA-PVA or

BuA-PVA, the reciprocal capacitance and the number of built-up films had linear relationships with a finite intercept. Since the Al_2O_3 layer and LB film formed on the Al electrode are serially connected, from the intercept in Figure 9, assuming a dielectric constant of 8, the thickness of the Al_2O_3 layer was determined from the slope of the curve was 3.7 for OA-PVA and 3.0 for BuA-PVA. For comparison purposes, it was determined that the spin-coating film of OA-PVA at the same temperature had a dielectric constant of 3.0, indicating that the value was higher in LB film.

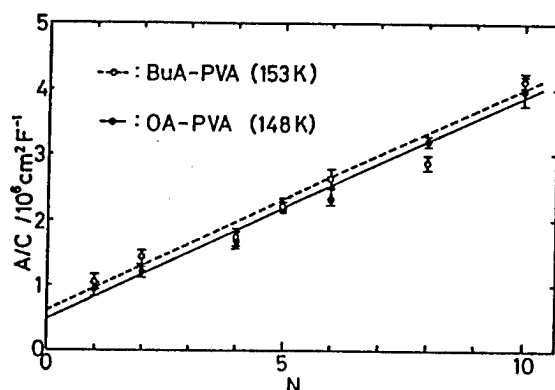


Figure 9. Relation Between Reciprocal Capacitance and Number of Layers

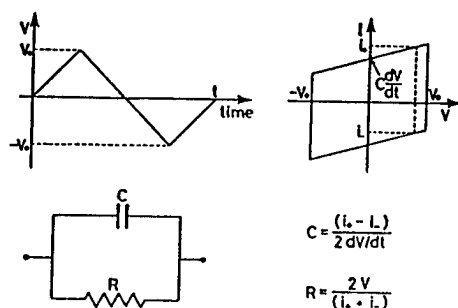


Figure 10. Method for Conductivity Measurements

The current response relative to DC voltage of the present insulation LB film showed a time dependency with a long relaxation time. Therefore, we determined the DC conductivity from the current response relative to triangular pulse voltage, as shown in Figure 10. Figure 10 shows a profile of current response relative to triangular pulse voltage. Assuming that the equivalence circuit of Al-LB film/Al is a parallel circuit of R and C, C and R can be obtained from the formulas shown in Figure 10. Since the resistance of Al and Al_2O_3 , contributing to the value of R, was significantly less than the resistance of LB film, the R value was assumed to be the resistance of LB film. The value of C obtained from the current value intercept was consistent with the capacitance obtained from the impedance analyzer.

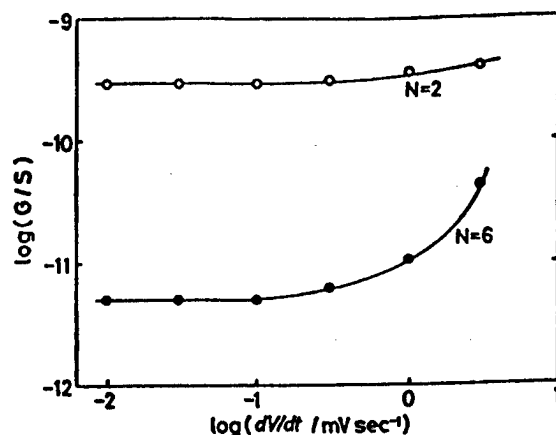


Figure 11. Conductance of Al/OA-PVA/Al at 148 K as a Function of Sweep Rate

Figure 11 shows the relationship between the sweep rate of the triangular pulse voltage and the cell conductance (G) in OA-PVA. Although the value of G was constant at a sweep rate of 0.1 mV/sec or less for a built-up film number of 2 or 6, at higher speeds the value tended to increase as the sweep rate increased. The increase in the value of G is apparently attributable to an increase in δ accompanying the Maxwell-Wagner-type surface polarization of the Al_2O_3 /polymer surface in this frequency region. The resistance of LB film was determined from measurements taken in the constant- G region, at 0.1 mV/sec or less, and DC conductivity was calculated. Similar patterns were also found in BuA-PVA, and its DC conductivity was calculated from measurements taken at 0.1 mV/sec or less.

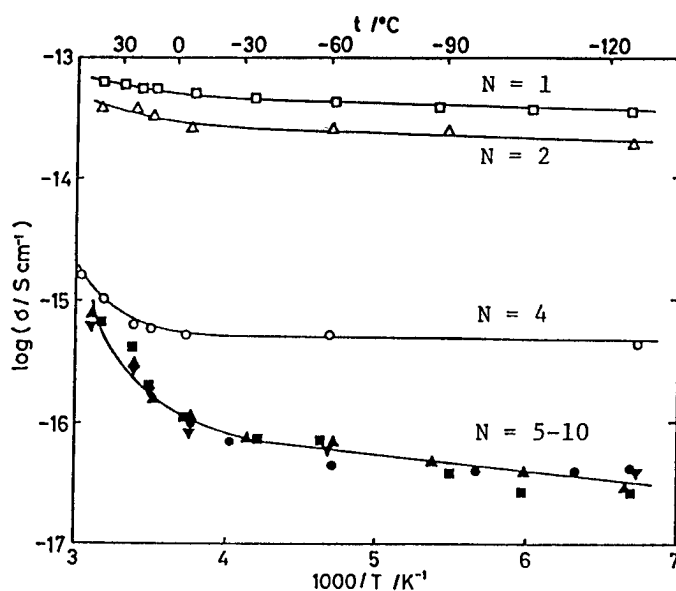


Figure 12. Temperature Dependence of Conductivity for Al/OA-PVA/Al

Figure 12 shows the temperature dependency of OA-PVA LB film DC conductivity. The DC conductivity of films with five layers or more (film thickness = 55 Å) converted to a certain value irrespective of the number of built-up films involved, and this conductivity agreed with the conductivity of spin-coating film. The sharp rise in DC conductivity around 10°C is thought to reflect a glass transition ($T_g = 32^\circ\text{C}$) of the sample. Also, near the glass transition temperature the conductivity was $10^{-17} - 10^{-16}$ S/cm, consistent with the conductivity of many insulating polymers. From these results, it appeared that in samples containing five layers or more the conductivity reflected bulk properties. In BuA-PVA, samples containing six layers or more exhibited the same behavior as that found in OA-PVA. In BuA-PVA, the sharp rise in DC conductivity occurred in the neighborhood of 40°C, reflecting a T_g (60°C) higher than the T_g of OA-PVA.

The conductivity of an OA-PVA LB film having four layers or less was significantly different from sample bulk properties in that it increased exponentially with decreases in the number of built-up films and showed little temperature dependency. The LB film with four layers had a constant conductivity relative to temperature up to about 20°C, beyond which it increased rapidly, apparently due to the fact that above 20°C the current flowing in the sample bulk had become dominant. Similar behavior was also observed in BuA-PVA having five layers or less.

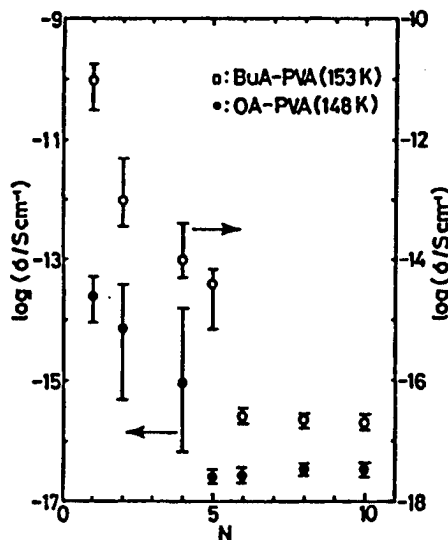


Figure 13. Conductivity of Al/Polymer/Al as a Function of Number of Layers

Figure 13 shows the relationships between the number of built-up films and conductivity in OA-PVA and BuA-PVA at a constant temperature. The conductivity of OA-PVA having five layers or more and that of BuA-PVA having six layers or more, both of which appeared to reflect sample bulk properties, showed a fair degree of reproducibility, attaining constancy of 10^{-17} S/cm conductivity regardless of the number of built-up films

involved. Samples having different methylene side chain lengths showed the same conductivity. In cases involving fewer built-up films, the variability in LB conductivity was of 1 to 2 orders of magnitude. Also, with decreases in the number of built-up films, conductivity increased exponentially. With the same number of built-up films, BuA-PVA and 1 to 2 orders of magnitude higher conductivity than OA-PVA did. The conductivity of monolayers was 10^{-14} S/cm for OA-PVA and 10^{-11} S/cm for BuA-PVA, lower than the 10^{-10} S/cm conductivity of a pure Al_2O_3 layer. The fact that in OA-PVA the conductivity was lower by 4 orders of magnitude seemed to indicate a high degree of coagulation of the two-dimensional polymer chains comprising the monolayers. The temperature dependency and built-up film number dependency of conductivity in LB films having a maximum of four layers (in the case of OA-PVA) or a maximum of five layers (in the case of BuA-PVA), and the differences between OA-PVA and BuA-PVA would seem to suggest that these properties are due to tunnel conduction. It is interesting to note that the critical film thickness at which bulk properties and tunnel current manifest themselves is approximately 40 Å for both OA-PVA and BuA-PVA.

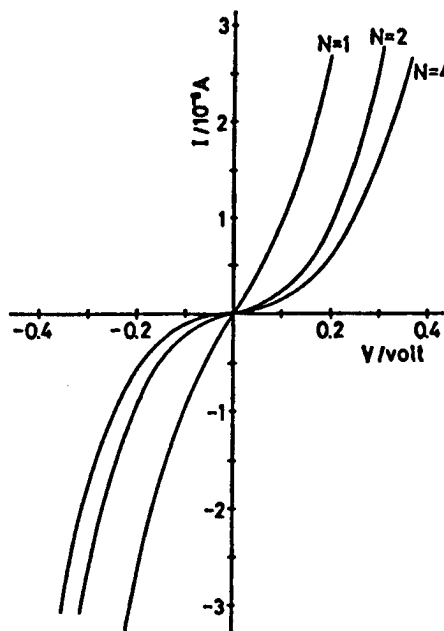


Figure 14. Current-Voltage Curves for Al/OA-PVA-Al at 148 K

We also investigated current responses at higher electric field intensities. Figure 14 shows the current-voltage curve (50 mV/min) for OA-PVA samples having one, two, and four layers. In the low voltage region (<0.05 V), j was proportional to V ; in the region between 0.05 and 0.1 V, j behaved non-ohmically; and above 0.2 V, the curve showed a characteristic tunnel conduction satisfying the relationship " (j/V^2) proportional to $1/V$." Figure 15 shows current-voltage curves (100 mV/min) of OA-PVA having five or six layers, which appear to show bulk properties. Compared with Figure 14, it is clear that the current-voltage curve changes rapidly in layers 4 and 5. Although the curve was more or less ohmic up to 1 V

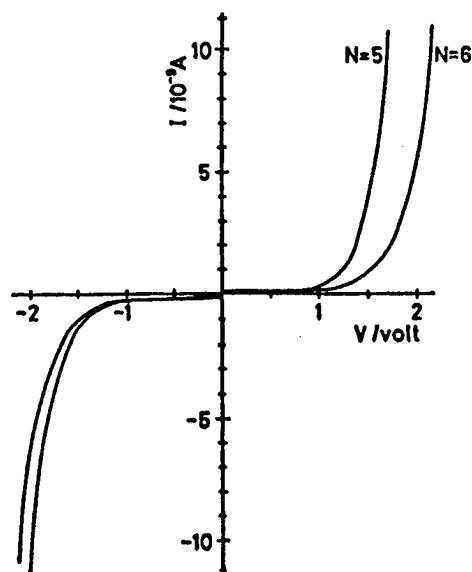


Figure 15. Current-Voltage Curves for Al/OA-PVA/Al at 148 K

(1.5 - 1.8 MV/cm), at higher voltage the current increased rapidly. The change in current as a function of voltage change was to a large extent reversible; a cyclic change in voltage showed current values which were virtually free of hysteresis. BuA-PVA samples having six layers or more also showed similar current-voltage curves.

5. Electrical Properties of LB Film on Chromium Substrate^{5,9}

In comparison with the properties of LB film on an aluminum substrate, since aluminum forms an Al_2O_3 layer, even an Al_2O_3 layer alone showed a conductivity free of temperature dependency, as shown in samples having 12 built-up films or less in Figure 12, or current-voltage characteristics as shown in Figure 14. Figure 16 shows the current-voltage characteristics of an $\text{Al}/\text{Al}_2\text{O}_3/\text{Al}$ junction using a naturally formed oxide film. We then investigated the electrical properties of LB film in which chromium, relatively immune to the formation of oxide layers and whose oxides have a high conductivity, was used as the base electrode. A cell made by allowing OA-PVA monolayers to build up on a chromium substrate and by vapor-depositing the upper aluminum electrode showed an ohmic current-voltage characteristic as long as the number of built-up films used was 30 or less; and the resistance of this cell was in fair agreement with the resistance of the cell without a film. From these facts, it was apparent that the electrodes were shorted. With a number 40 or higher built-up film, the aluminum electrode showed a current-voltage characteristic (Figure 15) indicative of bulk properties, as shown in Figure 17, and the temperature dependency of conductivity also agreed with that of films having five built-up films or more shown in Figure 12. The LB film on the chromium substrate, when the duration of vapor deposition on the upper aluminum electrode was reduced (to 15 seconds), formed a very thin, semitransparent electrode, and a tunnel conductivity-like characteristic emerged from the monolayers, as shown in Figure 18. The conditions employed

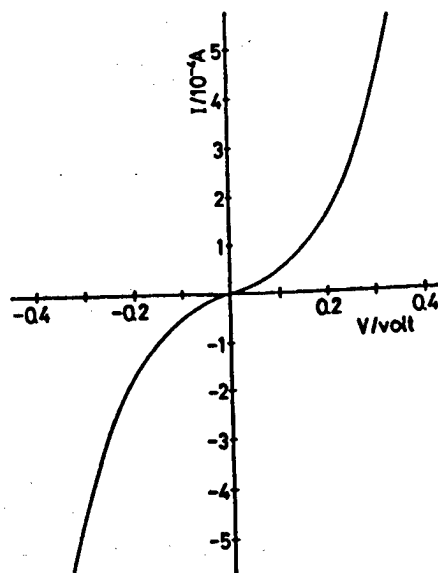


Figure 16. Current-Voltage Curve for Al/Al₂O₃/Al at 153 K

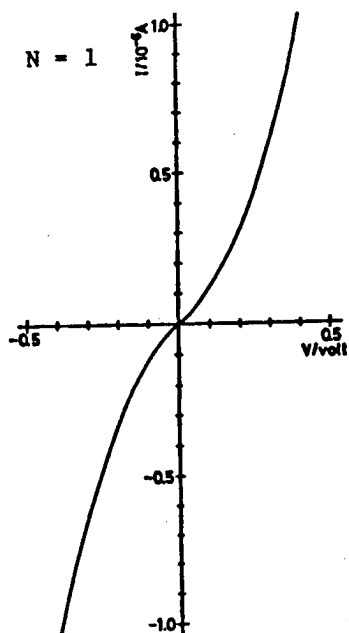


Figure 17. Current-Voltage Curve for Cr/OA/PVA/Al at 153 K

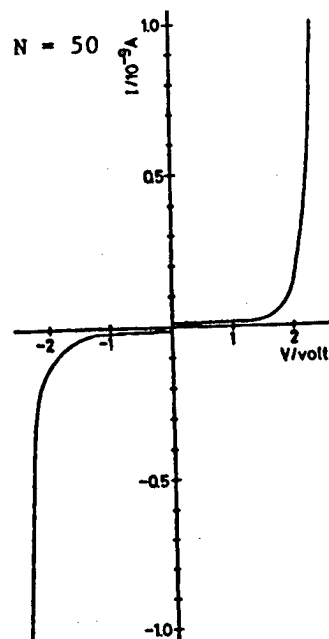


Figure 18. Current-Voltage Curve for Cr/OA/PVA-Al at 153 K

in vapor-depositing the upper aluminum electrode, with samples having 10 built-up films, showed a current-voltage curve similar to that shown in Figure 10.

The underlying causes of the significant differences in electrical properties between the LB film formed on a chromium substrate and that formed on an aluminum substrate are not yet understood. It is necessary to determine whether the differences are of a fundamental nature, reflecting the coagulation state of the LB film on the substrate, or reflecting differences in the coagulation state of polymer chains on chromium and aluminum; or whether they are due to a secondary factor such as short-circuiting through the electrode edges.

6. Concluding Remarks

In the foregoing, we have shown that application of the LB method to the formation of hydrophilic/hydrophobic polymers can yield polymer ultrathin films with controlled higher structures. A pressing need now exists for investigating the coagulation state of two-dimensional polymer chains comprising a polymeric LB film. A number of interesting problems still remain to be addressed; for example, the condition of gaps in polymeric LB films, such as those mentioned in this paper, as they relate to the frozen free volume in bulk, amorphous polymers existing on the glass state; and the question of whether the two-dimensional polymer chains in a monolayer exist at island-like aggregates or in a two-dimensionally intertwined state. Our knowledge of the electrical properties of polymeric LB films consists solely of empirical observations, and it is not understood whether or not these empirical data reflect the fundamental properties of the LB film. Much remains to be done in the future.

Acknowledgements

Part of the work presented herein was conducted jointly with Researcher Kiyoshi Koguchi of the Molecular Design Group (group leader: Kohei San-i), Ogata Fine Polymer Project, Research Development Corp. of Japan. Mr Koguchi's contributions are gratefully acknowledged.

References

1. K. Oguchi, T. Yoden, K. Sanui, and N. Ogata, POLYM J., Vol 18, 1986, p 877.
2. M. Watanabe, Y. Kosaka, K. Sanui, N. Ogata, K. Oguchi, and T. Yoden, MACROMOLECULES, Vol 20, 1987, p 452.
3. K. Oguchi, T. Yoden, Y. Kosaka, M. Watanabe, K. Sanui, and N. Ogata, to appear in THIN SOLID FILMS.
4. M. Watanabe, Y. Kosaka, K. Oguchi, K. Sanui, and N. Ogata, to appear in MACROMOLECULES.

5. M. Watanabe, Y. Kosaka, K. Sanui, N. Ogata, and K. Oguchi, POLYM. PREPR., JPN., Vol 36, 1987, p 3018.
6. Y. Fujiwara and S. Fujiwara, BULL. CHEM. SOC. JPN., Vol 37, 1968, p 1964.
7. See, for example: K. Shibatani, K. Fujii, Y. Oyanagi, J. Ukida, and M. Matsumoto, J. POLYM. SCI., Part C, Vol 23, 1968, p 647.
8. M. Watanabe, Y. Kosaka, K. Sanui, N. Ogata, K. Oguchi, and T. Yoden, POLYM. PREPR., JPN., Vol 35, 1986, p 2714.
9. M. Watanabe, Y. Kosaka, K. Sanui, and N. Ogata, Ibid., Vol 36, 1987, p 749.

20138/9365

Electrical Properties of Hydrophobic Polymer LB Films

43063801b Wako-shi BUNSHISEI CHOHA KUMAKU in Japanese Jan 88 pp 13-20

[Article by Atsutaka Shigehara, Polymer Chemistry, Riken Institute]

[Text] 1. Polymer LB Films

It appears that polymer LB films are superior to fatty acid (salt) LB films in mechanical properties and heat tolerance, offering a promise of wider applicability and greater yields during back-end processing, such as provision of metal electrodes by vapor deposition. It is for this reason that there has been a great deal of research in polymer LB films in recent years.

There are five ways of making polymer LB film:

- (1) Polymerization of low-molecular weight LB films
- (2) Polymerization of low-molecular weight LB films, followed by LB implementation
- (3) After-treatment of an LB film made of polymer precursors
- (4) Application of the LB method to a gaseous/liquid surface polymer film to make ultrathin films
- (5) LB implementation on a polymer itself

Although techniques (1) and (2) have been tried on fatty acids containing polymerizing unsaturated bonds, as a general rule introduction of unsaturated bonds results in lower T_c values for obtaining good quality LB films, and film formation by these techniques entails considerable technical hurdles. Also, these approaches give rise to new problems and questions such as stretching of films during polymerization, cleavage formation, and the question of whether or not the dynamic chain lengths (or real chain lengths) are appropriately distributed. Technique (3) has been successfully applied to the formation of polyimide LB films by after-treatment of polyamic acid long chain alkyl ammonium salt or polyamic acid alkyl ester LB film.^{1,2} However, this technique is liable to possible film defect formation during removal of either long chain alkyl amine or alcohol, and during the ensuing condensation and ring closure reactions. Technique (4), developed by Ogata, et al., affords an easy means of producing ultrathin films of heat-resistant polymers such as PBI (polybenzimidazol).³ Although still requiring improvements in the way of

adequate control over the degree of polymerization, the technique appears to have future growth potential. Technique (5) involves LB film formation by using the polymer itself; therefore, the polymer itself necessarily has to be soluble, a condition which imposes the limitation that LB film made in this manner can have a maximum of 300°C of heat tolerance. However, since the technique can be used with polymers of known molecular weight, molecular weight distribution, primary structures, and stereo regularity, LB films made from these polymers should have a high degree of uniformity. Also, since no after-treatment is involved, the technique entails little possibility of creating new film defects. Because of these advantages, in this symposium I shall discuss wet film formation using technique (5).

As a general rule, soft polymers containing vinyl main chains, such as polystyrene, exist in a solution as "hair balls" with intertwined polymer chains. Since LB films cannot be produced from "hair ball" polymers existing in the organic solution to be expanded in a water surface (since the film expanded on the water surface would be quite thick), it is necessary to provide a means of reducing interactions between polymer chains. There are three possible ways of accomplishing this goal: use of interpolymer chain electrostatic repulsion through introduction of an ionic hydrophilic base (α -olefin-MAN alternating copolymerization)⁴; introduction of a functional group offering "polymer-water" interaction, which is stronger than "polymer-polymer" interaction (partially acetalized PVA)⁵; and provision of nonflexibility through introduction of a stereo inhibitor group (polydialkylfumarate: alkyl = i - Pr, t-Bu, cyc-Hex).⁶ The first two approaches involve the use of hydrophilic polymer, which can accumulate on a hydrophilic aluminum or silicon substrate having an oxide layer on the surface. On the other hand, the third approach necessarily involves the use of a hydrophobic polymer, which can accumulate on a hydrophilic aluminum or silicon substrate having an oxide layer on the surface. On the other hand, the third approach necessarily involves the use of a hydrophobic polymer, which can accumulate on hydrophobic substrates such as Au and ITO.

2. LB Implementation of Polydialkyl Fumarate

Figure 1 shows the current-voltage characteristics of a metal-insulator-metal (MIM) device comprised of aluminum, cadmium salt of arachic acid (single layer), and aluminum.⁷ This well-known result demonstrated for the first time the existence of a tunneling effect through an LB monolayer film (I layer); also, because of the stability demonstrated by the LB film property despite the fact that a monolayer of cadmium salt of arachic acid measuring only 28 Å per layer was used, the graph has been thought to represent the uniformity of fatty acid LB films. However, although the conditions existing on the aluminum surface of the upper electrode (vapor-deposited) cannot be ascertained with a high degree of accuracy, it is expected that an oxide insulation layer extending as much as 30 to 70 Å exists on the aluminum surface of the lower electrode used during LB implementation. In fact, the current shown in Figure 1 is significantly less than the current which would be predicted if calculations were made by assuming an ϵ value of 2 to 3 and a thickness of 28 Å for the LB film, thus suggesting the existence of an Al₂O₃ layer about 40 Å thick. Since

specific evidence, such as an electron micrograph image of the cross-section, is lacking, the existence of this layer has not been proven; if it was the case that an LB insulation layer was overplayed on an oxide insulation layer, it would mean that we still do not have data indicating the properties of the LB film itself. It should be borne in mind that there has been a report⁸ indicating that if an Al_2O_3 layer is prepared with sufficient care (with an $\text{Al}/\text{Al}_2\text{O}_3/\text{Al}$ configuration), this layer alone can produce the tunneling effect.

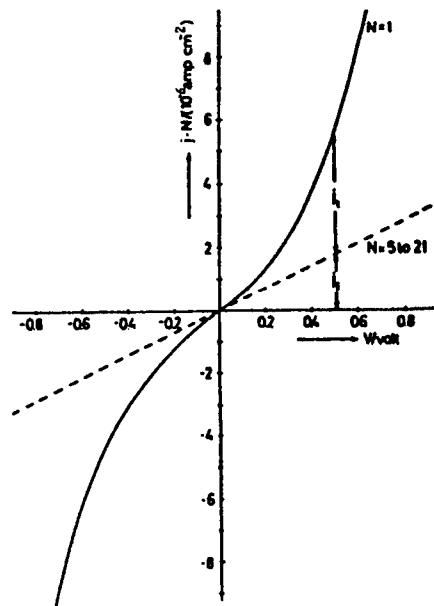


Figure 1. J-V Characteristics of (Al/arachic acid Cd-LB/Hg) MIM Device

It is probable that some of the film defects arising in a variety of LB processes, such as those due to chemical impurities in the LB material (LB substance itself or solvent), physical defects resulting from the LB fabrication process, or damage occurring during vapor deposition, are unavoidable. If leak current was present in MIM devices produced with utmost care to remove the causes of film defect, such leak current would be inherent in the LB film itself, and thus any hope of making an electric/electronic material solely from an LB film would have to be abandoned. The main purpose of the present research work is to investigate the presence of problems inherent in LB films.

When viewed from the conventional wisdom in polymer chemistry that α , β -bireplacement olefins (transisomers in particular) are difficult to polymerize by themselves, polydialkyl fumarate is an unusual polymer. Because of its peculiar structure, it was not until the beginning of the 1980's that the substance was polymerized to a high degree, through efforts by Otsu, et al.⁹ Table 1 lists the different types of polydialkyl fumarates used in the present investigation. Unless otherwise noted, we used a parent polymer as a source of PDiPF. As a rule, the polymer was dissolved in distilled chloroform in 0.5 - 1.0 mg/ml concentrations, and the

solution was expanded in purified water which had been treated by ion exchange, reverse osmosis, and double distillation. Also, unless otherwise noted, LB implementation was accomplished by transferring 20 dyn/cm of LB film onto 2.5 x 5 cm ITO (indium-tin oxide, 10 Ω /square, 0.2 - 0.251 μ m thick) (Nesa) glass or gold-deposited glass by vertical soaking at a rate of 6 mm/min at 21°C.

Table 1. Polydialkyl Fumarate

Alkyl group	Abbreviation	Note	Mn	Pn	Mw/Mn
i-Pr	PDiPF	parent polymer	12.4·10 ⁴	620	2.52
		Fr-1	72.0	3,600	1.13
		Fr-2	51.0	2,550	1.33
		Fr-3	38.9	1,950	1.17
		Fr-4	27.8	1,390	1.14
		Fr-5	19.0	950	1.14
		Fr-6	12.0	600	1.12
		Fr-7	6.8	340	1.29
		Fr-8	4.6	230	1.73
t-Bu	PDtBF	parent polymer	3.4	149	3.38
cyc-Hex	PDcHF	parent polymer	16.9	603	2.67

Figure 2 shows a plot of surface pressure-area-specific temperature (FA) curves for PDiPF, PDtBF, and PDcHF. All curves show a sharp rise reflecting a solid film formation, and indicate that film buildup can start at approximately 20 dyn/cm². These samples had limiting areas of 32 ± 1 , 34 ± 1 , and 38 ± 1 Å²/res., respectively.

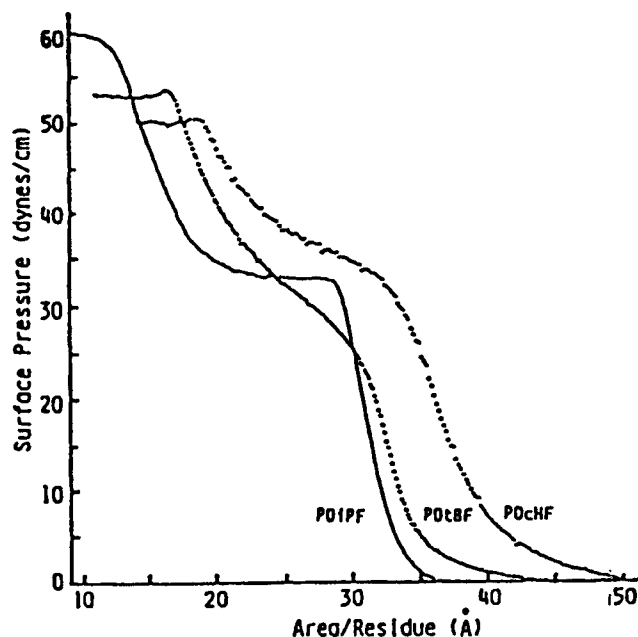


Figure 2. FA Curve for Polyfumarate (21°C, subphase: purified water)

With further increases in pressure, the curve rises again, reaching the collapsing point when the pressure exceeds the plateau region. This process is equivalent to the formation of two films on the water surface. Figure 3 shows FA curves of fractions 1-8 of PDiPF. Each sample had a limiting area size within the $32 \pm 1.5 \text{ \AA}^2$ range, with no molecular weight dependency. Figure 4 shows the temperature dependency of the FA curves; although not shown in the illustration because of the difficulty involved in maintaining a constant temperature, these samples had exactly identical limiting areas in the 60-80°C range, indicating that there was virtually no temperature dependency. Myristic acid (C_{14}), shown in the insert for comparison purposes, demonstrated an appreciable temperature dependency. Thus, to obtain a good-quality solid film state from myristic acid it would be necessary to maintain a constant temperature in the subphase to a considerable degree of accuracy, with a variation of less than 5°C. Thus, these two types of materials differ significantly in the ease with which LB films can be obtained.

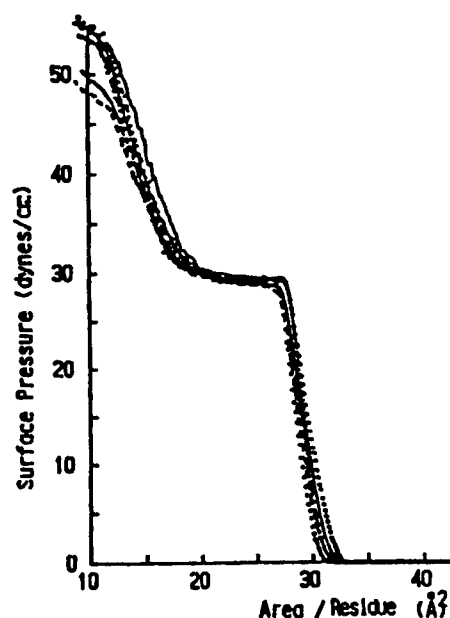


Figure 3. FA Curve for PDiPF of Different Molecular Weights (21°C, subphase: purified water)

Since polydialkyl fumarate has neither a dissociated group nor a specially hydrophilic group, its FA curve does not depend on the pH, inorganic ion species, or concentration in the subphase. For example, use of any of the following solution gives the same FA curve as that obtained by using purified water: HCl-NaOH at pH 1-12; MCl , $MClO_4$, MNO_3 , MCl_2 , $M(ClO_4)_2$, $M(NO_3)_2$, or $CuCl_2$ (where M stands for an alkali or alkali-earth metal ion) in 0 - 0.1 mol/l concentrations.

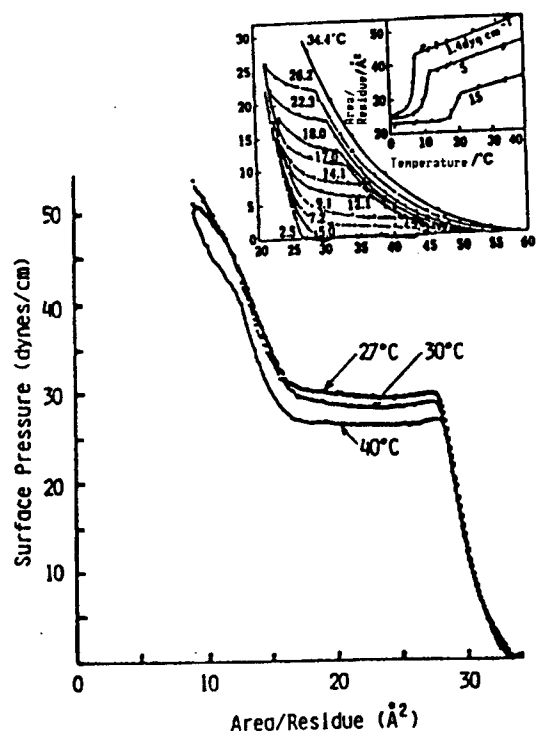


Figure 4. Temperature Dependency of FA Curves for PDiPF and Myristic Acid (insert)

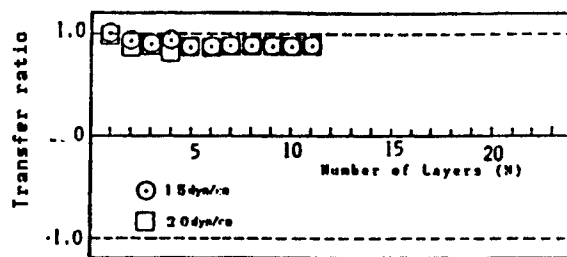


Figure 5. TR Value of PDiPF and Number of Vertical Soaking Strokes, Using an ITO Substrate

Figure 5 shows the relationship between the number of vertical soaking strokes used and the PDiPF accumulation ratio (transfer ratio: TR, with an odd number being the up-mode) obtained by using a TIO substrate. The decline in TR value from the second stroke on is attributable to the fact that the transfer of PDiPF in the first stroke somewhat lowers the meniscus position, thus reducing the effective surface area on the substrate. When this factor is taken into consideration, a TR value of $TR = 1.0 \pm 0.02$ is obtained. Figure 6 shows criteria for choosing a substrate for LB implementation of PDiPF by vertical soaking. On a hydrophilic substrate

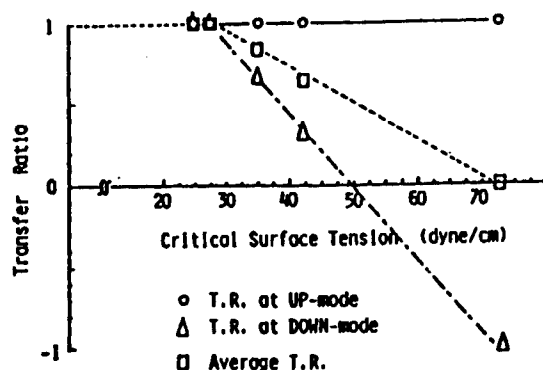


Figure 6. Substrate Surface Free Energy and TR Values

having surface free energy in excess of 30 dyn/cm, TR is approximately TR = 1 during the up-mode; however, in the following down-mode, it drops to -1 (all films peel off). When a somewhat hydrophobic substrate with a surface free energy value of 30 dyn/cm or less is used, TR remains TR = 1 during both up- and down-mode, so that film deposition is possible. Also, the horizontal adhesion method permits the use of almost any substrate, with the possible exception of teflon and other special materials.

LB films made on the ITO in this manner show no film defects that can be observed by condensation, differential interference micrography, or by combinations of these techniques. From surface roughness measurements on multilayer films, the thickness per layer was determined as 8.5 Å (PDiPF), 10 Å (PDtPF), and 12 Å (PDcHF); in particular, the thickness determination on PDiPF agreed well with the results of X-ray diffraction (9.1 ± 1.5 Å) and ellipsometry (8.7 ± 1.0 Å).

Figures 7 and 8 [not reproduced] show the planar polarization FT-IR of PDiPF powder (KBr) and LB film (gold-deposited substrate containing 305 layers). In Figure 7, there is considerable weakening of the C-H absorption band due to methyl groups, compared with carbonyl absorption, indicating that carbonyl groups are positioned perpendicular to the film plane and that C-H bonds are positioned approximately on the plane of the film. From calculations based on the limiting areas and the thicknesses of monolayer LB films, it appears that the LB film of PDiPF consists of long columns having elliptic cross sections (long axial diameter = 14 - 12 Å, monoaxial diameter = 8.5 Å), lying horizontally. From a molecular model assuming an energetically stable helical structure, the columns appear to consist of cylinders whose cross sections have a diameter of approximately 12 Å. When results of IR measurements are taken into consideration, it is possible that in an LB film the PDiPF has a zigzag-like structure with an elliptic cross section, rather than a helical structure with a round cross section. This question is now being investigated.

High-resolution electron microscopy could not be employed because of the possibility of destroying the sample; however, from differential interference optical microscope observations it is known that these films

do not have film defects at the submicron level or higher. As supplementary studies, we also carried out electrical property determinations, as described below.

MIM devices as shown in Figure 9 were prepared, and current-voltage (J-V) characteristics of monolayer PDiPF-LB films were measured (Figure 10). Compared with the data shown in Figure 1, these samples produced two orders of magnitude higher current values, indicating that the monolayer PDiPF-LB film was as thin as 8.5 Å; and in view of the nonlinear behavior of the J-V curve, the film's electrical conduction was clearly non-ohmic. Regarding these samples, it is necessary to determine whether or not the effects of leak current through the film pinholes can be removed.

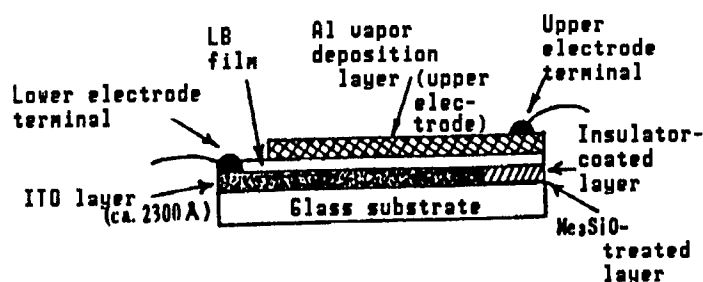


Figure 9. Configuration of the [ITO/PDiPF-LB/Al] MIM Device

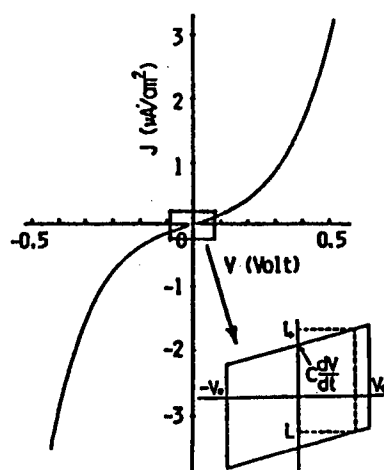


Figure 10. J-V Characteristics of an [ITO/PDiPF-LB(1L)/Al] MIM Device

At extremely low electric field intensities (i.e., less than ± 50 mV), the MIM device can be represented as a parallel circuit of condensers and resistors, which would give a J-C curve as shown in the insert in Figure 10. By using the following Equations (1) and (2), capacitance C and resistance R can be calculated. And, by using the relationships shown in Equation (3), N can be plotted relative to S/C ; from the slope of this curve the dielectric constant ϵ_s of the LB film can be obtained (Figure 11). In nonpolar polymers such as PDiPF, there should not be a

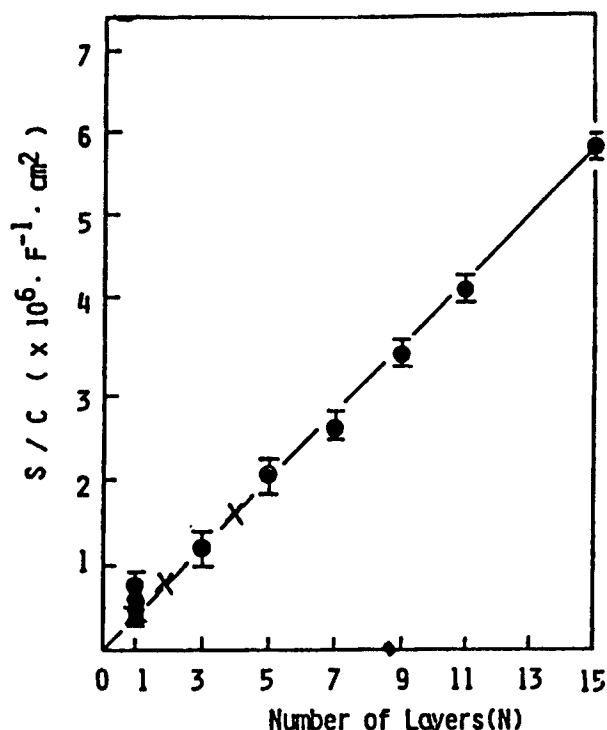


Figure 11. Reciprocal Capacitance Plot of an [ITO/PDiPF-OB(N-L)/Al] MIN Device

significant difference between its ϵ_s and the dielectric constant ϵ_s' of bulk solids. Therefore, if a comparison of ϵ_s and ϵ_s' indicates a fair degree of agreement, it will mean that the LB film has nonelectrically detectable defects. In particular, it is important that in S/C vs N graphs, plots representing a low number of layers do not deviate significantly from the straight line, since the presence of film defects would lead to short circuiting, especially when the number of layers involved is low, causing the 1/C points to occur above the straight line. Assuming a thickness of 8.5 Å per layer, and from the slope of the curve in Figure 10, ϵ_s has been calculated as 2.7 ± 0.35 , in good agreement with the value 2.65 for ϵ_s' for bulk solids (cast and spin-coat thick films). Also, the curve in Figure 10 passes through the origin, indicating that the first term on the right-hand side of Equation (3) is 0, i.e., $d_{ox} = 0$.

$$C = (I_+ - I_-)/(2dV/dt) \quad (1)$$

$$R = 2V_0/(I_+ + I_-) \quad (2)$$

$$S/C = (1/\epsilon_0)[(d_{ox}/\epsilon_{ox}) + (Nd/\epsilon_0)] \quad (3)$$

where ϵ_0 : dielectric constant of vacuum;
 ϵ_{ox} : relative dielectric constant of oxide layer;
 ϵ_s : relative dielectric constant of LB film;
 d_{ox} : thickness of oxide layer;
 d : thickness of LB film;
 N : number of LB layers.

Table 2 gives a summary of the mechanism of electrical conduction in layer I of the MIM device. If the nonlinear current response in Figure 10 is due to tunnel current, and if the thickness of layer I is fixed at a certain voltage value, Figure 10 gives a constant J. Also, Mann and Kuhn have calculated apparent conductivity σ from resistance R, which can be determined in the extremely low electric field region in Figure 10, and they have shown that the relationship indicated by Equation (4) holds between σ and the number of length layers, N.⁷ Therefore, if we allow the thickness of layer I to vary, apparent conductivity σ should decrease exponentially.

Table 2. Mechanism of Electrical Conduction in Insulators

Mechanism of electrical conduction	Equation	Voltage/temperature dependency
Schottky emission	$J = A^* T^2 \cdot \exp \{-q[\phi_B - (qE/4\pi\epsilon_1)^{1/2}]/kT\}$	$\sim T^2 \cdot \exp[aV^{1/2}/T - q\phi_B/kT]$
Fr.-Poole emission	$J \sim E \cdot \exp \{-q[\phi_B - (qE/4\pi\epsilon_1)^{1/2}]/kT\}$	$\sim V \cdot \exp[2aV^{1/2}/T - q\phi_B/kT]$
Tunnel or Field emission	$J \sim E^2 \cdot \exp[-4(2m^*)^{1/2}(q\phi_B)^{2/3}/3qhE]$	$\sim V^2 \cdot \exp(-b/V)$
Space-charge limited	$J = 8\epsilon_1 \mu V^2/9d^3$	$\sim V^2$
Ohmic	$J \sim E \cdot \exp(-\Delta E_{ae}/kT)$	$\sim V \cdot \exp(-c/T)$
Ionic	$J = (E/T) \cdot \exp(-\Delta E_{ai}/kT)$	$\sim (V/T) \cdot \exp(-f/T)$

A^* : effective Richardson constant; ϕ_B : barrier height; E : electric field; ϵ_1 : insulator electric permeability constant; m^* : effective mass; d : insulator thickness; ΔE_{ae} : energy of activation of electronic conduction; ΔE_{ai} : energy of activation of ionic conduction; $a = (q/4\pi\epsilon_1)^{1/2}$; $V = E \cdot d$; b, c , and f are constants independent of V and T .

$$\sigma(N) = \sigma_0 \cdot \exp(-2\alpha \ell \cdot N) \quad (4)$$

where ℓ : the thickness of a monolayer film potential barrier;
 α : (damping function) = $(2\pi/h)(2m\psi)^{1/2}$ $\sigma_0 = ae^2/2\pi h$;
 e : unit charge;
 ψ : effective barrier height.

Figures 12 and 13 illustrate the above relations. From these illustrations it is apparent that an LB film having a small number of layers gives a constant J irrespective of temperature (Figure 12), and that σ decreases exponentially as the number of LB layers increases (Figure 13). Thus, it appears that with an LB film having nine layers or less (approximately 80 Å) tunneling conductivity is dominant. The foregoing indicates that polyfuramate LB built-up films are usable as tunnel barrier layers. Applications of these films await future investigations.

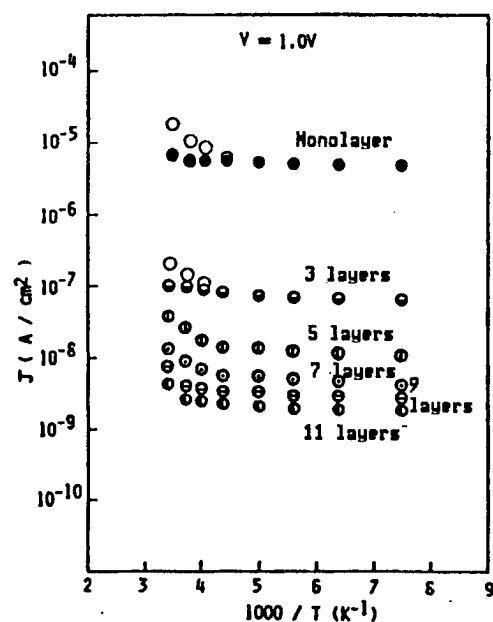


Figure 12. The Temperature Dependency of Quantity J of an [ITO/PDiPF-LB(N-L)/Al] MIM Device

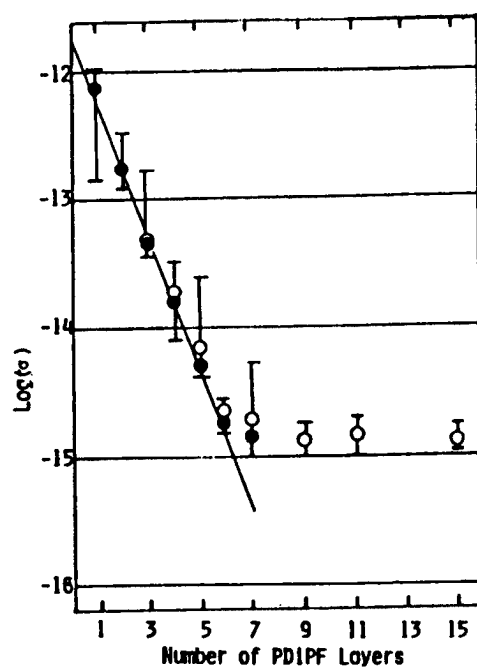


Figure 13. Dependency of Conductivity on Number of Layers in an [ITO/PDiPF-LB(N-L)/Al] MIM Device

References

1. M. Kakimoto, M. Suzuki, Y. Imai, M. Iwamoto, T. Hino, ACS Sympo., Ser. No 346, 1987, p 484; *idem.*, CHEM. LETT., Vol 395, 1987, p 823; Kakimoto, Nishikata, Imai, Spring Meeting of Japan Chemical Society, 3 IVA 46.
2. M. Uekita, H. Awaji, M. Murata, Third Int. Symp. on Mol. Elec. Devices, Arlington, 6-8 October 1986; Uekita, Awaji, Murata, Spring Meeting of Japan Chemical Society, 3 IVA 43.
3. A.K. Engel, Research Development Corp. of Japan, Synopsis of Ogata Fine Polymer Project Symposium, 6, 1986; Ogata, et al., 36th Polymer Symposium, Vol 36, 1987, Tokyo, p 3517.
4. R.H. Tredgold, C.S. Winter, THIN SOLID FILMS, Vol 99, 1983, p 81; R.H. Tredgold, Z.I. El-Badway, J. PHYS. D: APPL. PHYS., Vol 18, 1985, p 2483.
5. Koguchi, et al., 35th Polymer Symposium, 1986, p 2710; Watanabe, et al., *ibid.*, 1986, p 2714, 36th Polymer Symposium, 1987, p 3018.
6. Shigehara, et al., 35th Polymer Symposium, 1986, p 2542; 36th Polymer Symposium, 1987, p 3218; JACS, Vol 109, 1987, p 1237.
7. G. Mann, H. Kuhn, J. APPL. PHYS., Vol 42, 1971, p 4398; G. Mann, H. Kuhn, L.V. Szentpaly, CHEM. PHYS. LETT., Vol 8, 1971, p 82.
8. T. Nakayama, K. Mizushima, S. Egusa, M. Azuma, SYNTHETIC METALS, Vol 18, 1987, p 803; N. Gemma, K. Mizushima, A. Miura, M. Azuma, *Ibid.*, 1987, p 809.
9. N. Toyoda, T. Otsu, J. MACROMOL. SCI. CHEM., A19, 1983, p 1011.

20138/9365

SEM Observations of Biological Polymer LB Films

43063801c Wako-shi BUNSHISEI CHOHAKUMAKU in Japanese Jan 88 pp 21-28

[Article by Taiji Furuno, Biodevices, Riken Institute]

[Text] Using a scanning electron microscope (SEM), the author has investigated the structure of biological polymer LB films, with the following results:

- (1) It has been confirmed that a few layers of an LB film made of a synthetic polypeptide (PECG/MG) (Figure 1) can uniformly cover the surface of a granular ITO substrate.
- (2) Deterioration of purple films on the air/water surface and shrinkage of film fragments as a function of time were observed.
- (3) It was demonstrated that proteins measuring about 100 Å in diameter can be observed under SEM without requiring dyeing or vapor deposition treatments.

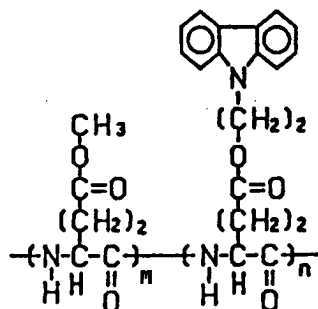


Figure 1. PECG/MG

Like amphipathic low molecules, granular proteins and enzymes, which are supposed to be water-soluble, can be made to float on a water surface. The history of LB film research indicates that as early as the second half of the 1930's the originator Langmuir studied the structures and activities of several enzymes by making them into monomolecular layers.^{1,2} By that time, several proteins had been crystallized, and there was growing recognition

that proteins might have regular structures. Also, sedimentation measurements indicated that water-soluble proteins were globular, and the low-angle X-ray diffraction techniques that came into being during the 1940's shed some light on the anisometry of their shapes. However, it was not until the advent of X-ray crystallography structural analysis by Perutz and Kendrew, and elucidation of protein structures at the atomic level, that the relationship between the structures and functions in enzymes came to be studied in detail. From the 1930's through the 1950's, research on protein monomolecular films was driven by interest in surface chemistry and biochemistry. Specifically, among the questions pursued was: given that proteins undergo denaturation at air or water surface, transforming themselves to a film about 10 Å thick, if an enzyme was put in that condition, to what extent might its enzyme activity be affected? Up to the 1950's, the argument went something like this: 1) expansion of hydrophilic proteins on the water surface results in some loss of the proteins to the water; 2) unlike the small molecules, expanded proteins undergo a change in their film structure over a long period of time; 3) the film structure at the surface depends on the degree of expansion³; and 4) different types of proteins behave differently on the surface. Thus, the argument was rather confusing, and this state of affair has not significantly changed even now.

Aside from surface chemistry or biochemistry, it was thought that development of techniques for freely inducing two-dimensional crystallization of proteins would significantly aid the advancement of protein structure research. Such techniques would also form an important basis for the development of a future protein or enzyme-based device technology. Probably the air/water interface would be one of the best settings in which such devices might be realized. To accomplish this goal, it would be necessary to develop a means of inhibiting protein denaturation at the surface. The crystallization technique using a lipid monomolecular film stretched on the air/water surface and crystallization using adsorption to lipid double films provided on a substrate would seem to constitute important breakthroughs in recent research.^{4,5,6} It seems that the base for these accomplishments had been constructed by research on surface films conducted before the 1950's. Specifically it had come to be known that a protein adsorbing from the water phase to the protein monomolecular film denatured on a surface tends to retain its activity and does not undergo large structural changes,³ and that the lipid monomolecular film on the water surface and proteins interact, in some cases the proteins invading the lipid film.⁷ Although the techniques based on the adsorption of proteins to a lipid film seems to represent a significant advancement toward two-dimensional protein crystallization, it would be difficult to predict that eventually it should be possible to crystallize any protein by this method. The reason is that the method involves mixing ligands in the lipid film as preparatory to crystallization, and that once a protein adsorbs itself on a ligand, it moves around two-dimensionally in the film before it starts crystallizing. Furthermore, although the method is exceedingly simple, it is at the mercy of many factors governing crystallization: temperature, time, pH, ionic strength, surface pressure, ligand concentration, and the type of lipid used. Therefore, the success of the method is largely dependent on the

experimenter's intuition and a process of trial and error. It would seem that the use of this method requires a means of assessing the degree of packing of protein molecules on a routine basis, albeit at low resolution, in a manner which is not necessarily intended for structural analysis.

Until now, the only available means of viewing the structure of a protein two-dimensional crystal as a real image has been the transmission electron microscope. However, the author has confirmed that the same purpose can also be accomplished by using a high-resolution SEM (specifically, the S900 made by Hitachi, Ltd.). As a rule, it is possible to observe the degree of protein packing on any conducting substrate without requiring any special treatment. Although a metal vapor deposition substrate might seem a logical choice as the substrate to be used, none of the thermal vapor deposition, ion coating, or electron beam thermal vapor deposition substrates has had a grain size fine enough for observing protein shapes. Although silicon wafers containing a naturally formed oxide film on the surface are normally used as structures, even these are not sufficiently smooth. It seems that the use of graphite and other monocrystals should be tried.

1. Uniformity of Polypeptide LB Films on an ITO

The polypeptide LB film shown in Figure 1, exhibiting photoconductivity, is of considerable interest from a physical property standpoint; however, in the following we shall focus on its structure, and particularly its structure on an ITO substrate. The base ITO used in this research, as shown in Figure 2 [not reproduced], is an aggregate of particles measuring 3-40 nm in diameter. Accumulation of PEGG/MG LB films on such a base gives rather low yields when the number of layers used is one to three. However, despite its low yields the method served to indicate a relationship between resistivity and the number of layers involved, as shown in Figure 3. For comparison, arachic acid was accumulated on the ITO substrate, and current-voltage characteristics were measured using aluminum as the upper electrode. The results indicated that in all cases involving 15 layers or less, the layers were electrically short-circuited. When creating an arachic acid LB film on a glass substrate, as a general rule bivalent ions are added to the water phase in order to stabilize the monomolecular films and facilitate their accumulation. Although it is held that improvements in film quality can be obtained in CaBaCd order, as far as could be ascertained during the present research the addition of Ca or Cd ions did not yield good quality films. Many defects were observed under the Nomarski microscope. Figure 4 [not reproduced] shows an SEM image of these defects. It can be seen that films have peeled off and have become globs, baring the base structure in the periphery. In the presence of barium ions, by maintaining a somewhat low aqueous phase pH, films free of defects that can be seen under the Nomarski microscope could be obtained (Figure 5 [not reproduced]). In Figure 4 [not reproduced], although no globs are visible, the base structure is clearly visible, and there are many bright, shiny ITO particles in view. Even if these particles are not completely exposed, clearly the base material does not have 15 layers of arachic acid built upon it. If aluminum is vapor-deposited as an upper electrode, these spots of exposed base material are likely to produce short circuit paths.

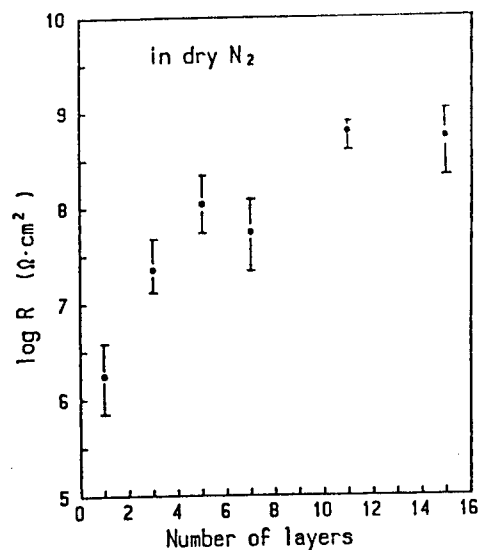


Figure 3. Relationship Between the Resistivity of ITO [PECG/MG LB Film]Al Sandwiched Cells and the Number of Layers

it is interesting to note that the thickness of an LB film having 15 layers is approximately equal to the maximum diameter of ITO particles. By contrast, ITO particles are uniformly covered by PECG/MG LB, as shown in Figure 6 [not reproduced], and there are few spots where the base material is exposed. It is thus clear that the uniformity of film contributes significantly to the degree of film insulability.

2. Surface Denaturation of Purple Film

Purple film is a two-dimensional crystal of a film protein called "bacterio-rhodopsin" (bR).⁸ A film fragment is 45 Å thick and has a diameter of approximately 0.5 μm. Being reasonably heat-stable, the material is capable of retaining its crystalline structure up to 80°C.

By gently discharging a suspension of purple films onto the water surface in the presence of bivalent ions in 10⁻³M concentrations, film fragments can be made on the gaseous/aqueous surface. Films made in this manner, however, showed a behavior substantially different from the behavior that would be expected from an aggregate of stable film fragments. As shown in Figure 7, for example, when compression was started 2 hours after the expansion, and when area-pressure curves were measured, with an initial coverage rate of 0.28, pressure was observed in the neighborhood of 3,600 Å²/bR. This value is approximately three times higher than the area that would be occupied by molecules if the bR had a crystal structure within the purple film. This ratio can be increased to a fourfold difference by further increasing the waiting time after the expansion. Also, when the film fragments were held in a constant surface area by setting the initial coverage rate at 0.8, natural surface pressure set in, reaching approximately 8 dyn/cm. These results are analogous to surface denaturation of water-soluble proteins.

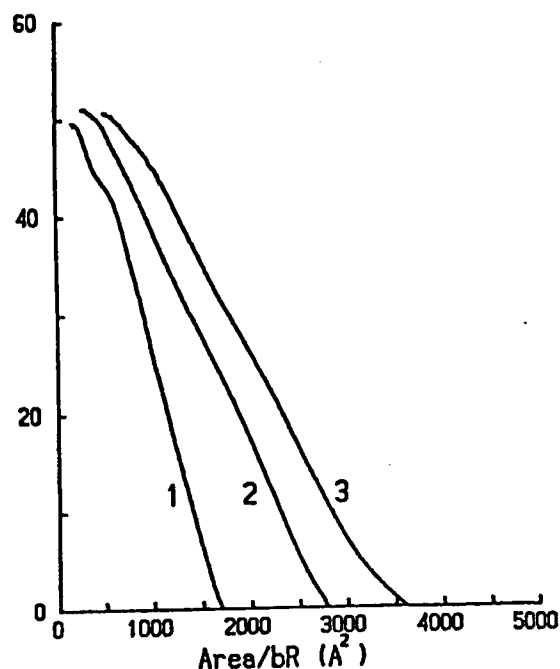


Figure 7. The π -A Curve of Purple Film Monolayer
 Compression was started 2 hours after expansion. Initial coverage rates: 1, 0.68; 2, 0.41; 3, 0.25

To establish the presence or absence of surface denaturation of purple film in terms of a change in film fragment shape, we transferred the purple films expanded on the water surface to a silicon substrate, and observed them under SEM. Figure 8 [not reproduced] shows film fragments transferred by using a surface pressure of 15 dyn/cm. Figure 8(a) indicates the film fragments transferred after a 30-minute wait; Figure 8(b) indicates the film fragments transferred after a 5-hour wait. Films that have been allowed to stand on the water surface for such a long time show decreases in both film fragment size and density. Given that a surface pressure of 1 dyn/cm was employed, it is difficult to imagine film fragments having the distribution pattern shown in Figure 8(b), in which there is no substance occupying the space between film fragments. SEM observations of such space by several methods indicate that the space between film fragments is occupied by a type of film different from the purple film. Accumulation of surface films after letting the films stand until there are few remaining film fragments, and the results of SDS-acrylamide-gel electrophoresis analyses indicates that the LB film as a whole contains bacterio-rhodopsin in the amount expected.

These results indicate that even if the purple film is thermally stable, on the substrate surface the material undergoes denaturation, starting at the periphery, and dissolving in the solvent.

Relating to its function as a proton pump, the purple film has distinct front and back sides. These sides differ in the number of surface

dissociating amino acids which they contain. On the gaseous or aqueous surface are purple films facing up or down; are they randomly oriented, and if not, to what extent are they lined up?

These are some of the questions that need to be answered in the future. Also, given that a purple film is a film fragment about 1 μm wide, would it be possible to use these fragments so that a substrate surface could be covered completely with a single sheet of purple film? Liposome and cells are capable of fusing substances. Likewise, there is a possibility that we may be able to fuse purple film and control their growth.⁹

3. Monolayers of Ferritin and Apoferritin

Concerning the monolayers of ferritin and apoferritin, the author is conducting research from two standpoints: 1) what degree of packing of these monolayers can be achieved by direct expansion to the water surface without using lipid film adsorption methods⁴⁻⁶; and 2) whether or not SEM affords an effective means of studying the degree of packing of these films or their surface denaturation.

As a protein, ferritin has a molecular weight of approximately 440,000; it has a spherical shell structure with an outer diameter of 13 nm and inner diameter of 7.5 nm; in the interior of its structure, ferritin has an accumulation of 4,500 iron atoms in the form of oxides.¹⁰ The substance created by removing the iron oxide core from ferritin, making it into an outer shell protein, is known as apoferritin. As with the case of creating ordinary LB films, apoferritin can be expanded to the aqueous phase surface of low ionic concentrations. Under these conditions ferritin would be lost almost completely to the aqueous phase; however, it can easily be expanded to the surface of ammonium sulfate or sodium sulfate at 1 M or higher concentration.

Because it contains a large number of iron atoms in its interior, ferritin offers high secondary electron generation efficiency, and on a silicon substrate ferritin can be seen as particles brighter than the base material. Figure 9 [not reproduced] shows an SEM image of ferritin obtained by expanding an excess amount of the substance on a 1 M sodium sulfate solution containing 0.1 percent glutaraldehyde, letting it stand for 24 hours under equilibrium surface pressure, and transferring the results to a silicon substrate. The illustration shows dense packing of globular ferritin molecules.

The author has investigated the structure of apoferritin on a salt solution of low salt concentration (CaCl_2 , 0.4 mM). When a film was obtained by compressing it immediately after expansion, and by transferring the film to a substrate, apoferritin particles were seen to be distributed at a low density, with few apoferritin particles sticking together. The particle sizes were 15-20 nm, larger than those found in aqueous solutions, probably due to the fact that the globular structure of apoferritin did not survive the drying process. By contrast, a film obtained by transferring it immediately after expansion under high surface pressure (25 dyn/cm) formed a mesh structure with an aggregation of apoferritin particles, as shown in

Figure 10(a) [not reproduced]. The gaps in the mesh were not just space; they showed light and dark patterns which appeared to have been derived from apoferritin. The fiber thickness corresponded to 1 to 3 molecules, and in some locations even larger aggregates were present. In the SEM images, the particular shape of the apoferritin molecules cannot be distinguished clearly. Apparently the thick fiber structure was a transient structure, which changed into an aggregation of highly dense globular particles in a matter of a few minutes.

In contrast, Figure 10(b) [not reproduced] shows a film created by enlarging the surface area after expansion, reducing the surface pressure to zero, letting it stand for 1 hour (with the surface pressure rising to 2 dyn/cm), compressing the area to 25 dyn/cm again, then transferring the film to harvest it. The image clearly shows that apoferritin has a low density, with fiber diameters so narrow that the fibers are difficult to distinguish. In areas not occupied by fibers or clearly visible particles, the space is occupied by more fine fiber-like structures than the number of these structures present in Figure 10(a). These results would seem to suggest that on the water surface the molecules undergo denaturation (untied) with the passage of time. When high surface pressure (e.g., > 20 dyn/cm) was maintained after compression, time-dependent structural changes (denaturation) could not be seen with any degree of clarity. This suggests, conversely, that maintaining high surface pressure inhibits surface denaturation.

Thus, it has been demonstrated that with larger proteins the external shapes and packing of protein particles can be observed clearly under SEM, and that patterns of surface denaturation can be evaluated in this manner.

The foregoing indicates that because of its high resolving power, the SEM method, until now employed mainly for the purpose of observing tissues in biological samples, can be used effectively as a means of routine checking of protein shapes and packing states. Before the technique can be put to practical use, however, a number of problems need to be resolved, such as the preparation of base substrates, avoiding contamination, and avoiding sample damage from the electron beam. Also, further work is needed to improve the quality of protein imaging under SEM. There is a possibility that physically oriented methods for two-dimensional crystallization of proteins might be developed in the future.

Although the topic was not mentioned in the foregoing, on-the-spot observation of proteins by epi-illumination fluorescent microscopy may contribute significant to research on the gaseous or aqueous surface films of proteins. Originally this method was employed for elucidating the relationship between the film structure and the pressure change accompanying compression, by doping a fluorescent dye in a lipid film. The method allows observation of fluorescent or fluorescence-labeled proteins, provided these proteins form micron-level structure on the water surface.¹¹ If correspondence between the micron-level structures observed by this method and the angstrom-level structures under an electron microscope could be established, the epi-illumination method might furnish useful information for two-dimensional crystallization of proteins.

References

1. I. Langmuir and V.J. Schaefer: J. AMER. CHEM. SOC., Vol 60, 1938, p 1351.
2. Ibid., CHEM. REV., Vol 24, 1939, p 181.
3. L.G. Augenstein, C.A. Ghiron, and L.F. Nims, J. PHYS. CHEM., Vol 62, 1958, p 1231.
4. E.E. Uzgiris and R.D. Kornberg, NATURE, Vol 301, 1983, p 134.
5. D.S. Ludwig, H.O. Ribi, G.K. Schoolnik, and R.D. Kornberg, Proceedings Natl. Acad. Sci., Vol 83, 1986, p 8585.
6. E.E. Uzgiris, BIOCHEM. J., Vol 242, 1987, p 293.
7. P. Doty and J.H. Schulman, Discuss. Faraday Soc., Vol 6, 1949, p 21.
8. R. Henderson, J. MOL BIOL., Vol 93, 1975, p 123.
9. D. Neugebauer, H.P. Zingsheim, and D. Oesterhelt, J. MOL. BIOL., Vol 123, 1978, p 247.
10. S.H. Banyard, D.K. Tammers, and P.M. Harrison, NATURE, Vol 271, 1978, p 282.
11. W.M. Heckl, M. Losche, and M. Mohwald, THIN SOLID FILMS, Vol 133, 1985, p 73.

20138/9365

Optical Recording Properties of Naphthophthalocyanine Film

43063801d Wako-shi BUNSHISEI CHOHAKUMAKU in Japanese Jan 88 pp 29-38

[Article by Toshiyuki Sugano, Olympus Optical Co., Ltd.]

[Text] 1. Introduction

Increasing use of information technologies requires a means of processing masses of a wide variety of information quickly and efficiently. This, in turn, requires memory devices capable of recording large volumes of information accurately, quickly, and at low cost. Magnetic memory, until now the mainstream of memory technology, may prove increasingly inadequate in terms of recording density and cost.

Recent rapid progress in optoelectronics technology (semiconductor laser, servo, and media development technologies) and anticipated increases in surface recording densities¹ have stimulated interest in optical memories because of their potential for realizing high-capacity low-cost, compact, and high-density data storage.

Active research is being conducted on optical recording media; initially much of the effort was directed at metal films based on tellurium (Te-C, Te-CS₂, Te-Ox, Te-Se), but, recently organic polymer recording media have been gaining attention because of following advantages:

- (1) The possibility of molecular design according to light source wavelength and recording method requirements to attain high light absorption coefficients.
- (2) Excellent thermal properties (low melting point, low decomposition point, and low thermal conductivity).
- (3) Ease of film formation.
- (4) Freedom from rusting and cracking, contrast to metals.
- (5) Low toxicity.

These advantages offer the potential for achieving: 1) high sensitivity; 2) high recording density; 3) lower process cost; 4) improved corrosion resistance; and 5) low toxicity.

2. Organic Pigment Recording Media and Underlying Recording Principles

Recording on media consisting of organic pigments can be accomplished either by heat mode, in which light is converted to heat, or photon mode, based on photon-induced photochemical reactions (isomerization). Currently most of the practical organic recording media are based on the heat mode; in the future, the photon mode is likely to be the mainstream memory technology.

This paper will discuss the types of hole drilling that can be realized in the heat mode (Figure 1).²⁻⁷

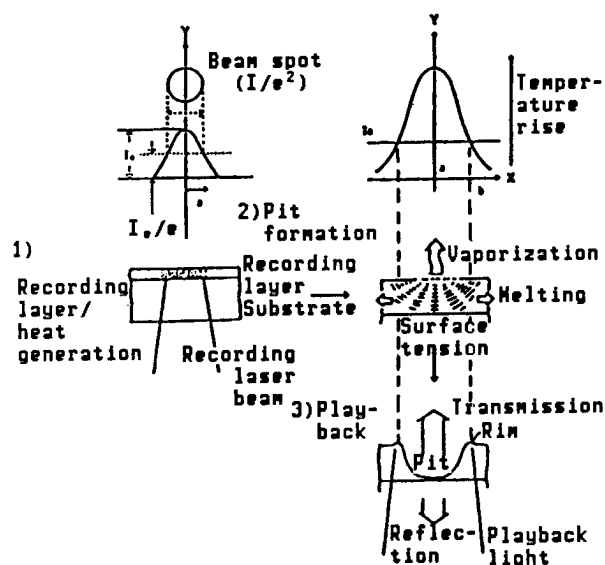
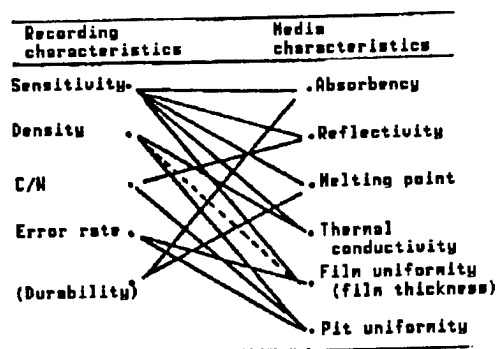


Figure 1. Principle of Pit Formation

The recording principles employed involve directing the laser beam, modulated by input signals, to a recording film through a substrate, and irradiating the recording film in order to induce physical/chemical changes on the film through melting, sublimation (vaporization), or changes on surface tension, thus producing pits.

To ensure adequate recording characteristics in the medium, the pigments shown in Table 1 must be capable of efficient light absorption and most readily undergo either melting or sublimation, in order to form pits.

Table 1. Recording Characteristics and Necessary Media Characteristics



High reflectivity on the recording film ensures large optical modulation between the pit and nonpit parts of the film, thus increasing the playback sensitivity (S/N). Furthermore, the pigment must be sufficiently light-tolerant in order to permit repeated playback actions, must offer adequate heat and humidity tolerance to permit long-term storage, and must be free of pigment crystallization, coagulation, and other changes of state during film fabrication.

Table 2. Examples of Known Pigments

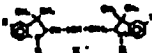

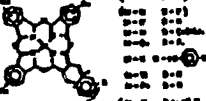
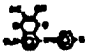
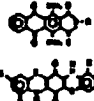
Constituent compound	Structural formula	λ _{max} (nm)	ε _{max}	Source
Cyanine		~680	80 ~	Ricoh Sica-air TOK Olympus
Squali-rum				Phillips Sany IBM
Phthalo-cyanine	 λ_{max} (nm): 620, 630, 640, 650, 660, 670, 680, 690, 700, 710, 720, 730, 740, 750, 760, 770, 780, 790, 800, 810, 820, 830, 840, 850, 860, 870, 880, 890, 900, 910, 920, 930, 940, 950, 960, 970, 980, 990, 1000 ϵ_{max} : 100, 110, 120, 130, 140, 150, 160, 170, 180, 190, 200, 210, 220, 230, 240, 250, 260, 270, 280, 290, 300, 310, 320, 330, 340, 350, 360, 370, 380, 390, 400, 410, 420, 430, 440, 450, 460, 470, 480, 490, 500, 510, 520, 530, 540, 550, 560, 570, 580, 590, 600, 610, 620, 630, 640, 650, 660, 670, 680, 690, 700, 710, 720, 730, 740, 750, 760, 770, 780, 790, 800, 810, 820, 830, 840, 850, 860, 870, 880, 890, 900, 910, 920, 930, 940, 950, 960, 970, 980, 990, 1000	24.3 17.0	Ricoh ICI MIT TOK Olympus	
Naphtha-quinone	 λ_{max} (nm): 400, 410, 420, 430, 440, 450, 460, 470, 480, 490, 500, 510, 520, 530, 540, 550, 560, 570, 580, 590, 600, 610, 620, 630, 640, 650, 660, 670, 680, 690, 700, 710, 720, 730, 740, 750, 760, 770, 780, 790, 800, 810, 820, 830, 840, 850, 860, 870, 880, 890, 900, 910, 920, 930, 940, 950, 960, 970, 980, 990, 1000 ϵ_{max} : 100, 110, 120, 130, 140, 150, 160, 170, 180, 190, 200, 210, 220, 230, 240, 250, 260, 270, 280, 290, 300, 310, 320, 330, 340, 350, 360, 370, 380, 390, 400, 410, 420, 430, 440, 450, 460, 470, 480, 490, 500, 510, 520, 530, 540, 550, 560, 570, 580, 590, 600, 610, 620, 630, 640, 650, 660, 670, 680, 690, 700, 710, 720, 730, 740, 750, 760, 770, 780, 790, 800, 810, 820, 830, 840, 850, 860, 870, 880, 890, 900, 910, 920, 930, 940, 950, 960, 970, 980, 990, 1000	700 710	1.00 1.07	NEC
Anthra-quinone	 λ_{max} (nm): 400, 410, 420, 430, 440, 450, 460, 470, 480, 490, 500, 510, 520, 530, 540, 550, 560, 570, 580, 590, 600, 610, 620, 630, 640, 650, 660, 670, 680, 690, 700, 710, 720, 730, 740, 750, 760, 770, 780, 790, 800, 810, 820, 830, 840, 850, 860, 870, 880, 890, 900, 910, 920, 930, 940, 950, 960, 970, 980, 990, 1000 ϵ_{max} : 100, 110, 120, 130, 140, 150, 160, 170, 180, 190, 200, 210, 220, 230, 240, 250, 260, 270, 280, 290, 300, 310, 320, 330, 340, 350, 360, 370, 380, 390, 400, 410, 420, 430, 440, 450, 460, 470, 480, 490, 500, 510, 520, 530, 540, 550, 560, 570, 580, 590, 600, 610, 620, 630, 640, 650, 660, 670, 680, 690, 700, 710, 720, 730, 740, 750, 760, 770, 780, 790, 800, 810, 820, 830, 840, 850, 860, 870, 880, 890, 900, 910, 920, 930, 940, 950, 960, 970, 980, 990, 1000	700 710	0.7 0.7	Ricoh

Table 2 presents a roster of representative organic pigment used in optical memory media.⁸ Since around 1981, there have been large numbers of published papers and patent disclosures in the field of optical memory media. Among these pigments, polymethylene cyan pigment and (naphtho)phthalocyanin pigment are the most popular.

Between these two types of pigments, the (naphtho)phthalocyanin family of compounds, although inferior in optical, thermal, and melting properties, are superior to metallic pigments in resistance to optical degradation and environmental tolerance (Figure 2).

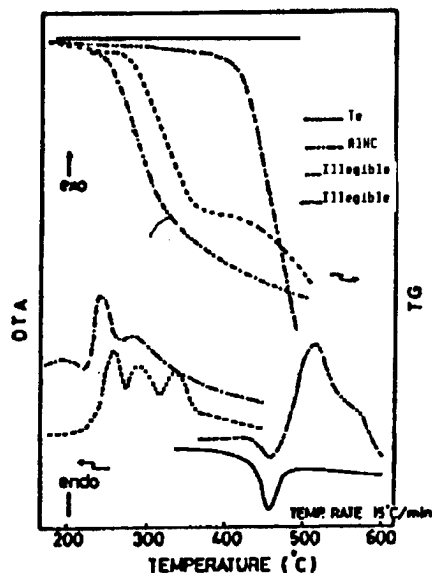


Figure 2. Pigment TG/DTA Characteristics

3. Naphthophthalocyanine-Based Pigments

(Naphtho)phthalocyanine pigment has the structural formula shown in Figure 3. It has an absorption region on the long wavelength side. It is widely used as a cosmetic pigment excelling in light, humidity, and heat tolerances. Also, as presented in the 1986 symposium of this program, it has been gaining attention as a functional pigment offering photoelectric, electrical, and catalytic properties. To realize these functions in a device requires formation of a thin film with the appropriate molecular layout.

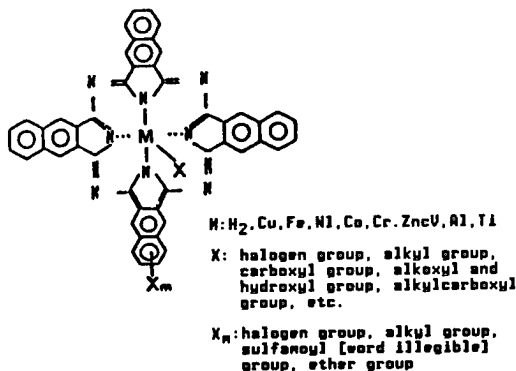


Figure 3. Structural Formula

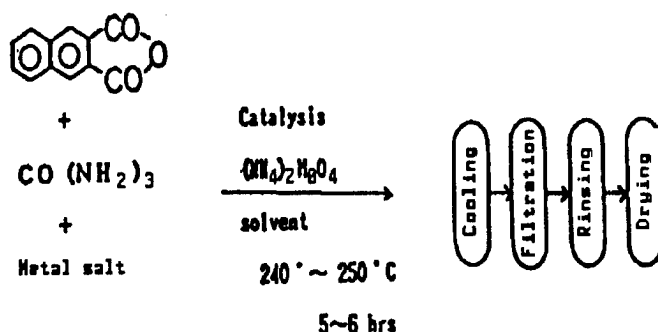
Because of its sublimation propensity, (naphtho)phthalocyanine pigments have been used in vacuum vapor deposition, molecular beam vapor deposition, and other dry methods for film formation. Also, in view of the fact that the solubility of these pigments can be improved by X and X_m substitutions, Shigehara, et al., have introduced an alkoxy group into the X_m site to achieve thin film formation by the LB method. Furthermore, in the type of heat mode optical recording films presented herein, soluble substitution groups have been introduced into the X and X_m sites, and thin films have been formed by the spin-coating method to achieve practical utilization, as

proposed in the following patent disclosures: S-61-268487, 62-56191/Mitsui Toatsu, 61-177281, 61-177288/Celanese, 61-25886/Yamamoto Chemical Synthesis, and 61-197280/TDK. This paper will discuss the optical recording properties of recording films made by vacuum vapor deposition.

4. Molecular Structure and Optical Recording Properties of Naphthophthalocyanine

Naphthophthalocyanine can be synthesized by the Wyler or imide method. For the purposes of our work, we have used samples made by Wyler synthesis. As is known, the physical properties of this substance are subject to variations according to the particular synthesis conditions and after-treatment conditions employed.

Synthetic method
Wyler method



The following vapor deposition conditions are employed for film formation:

Film state	Degree of vacuum	Approximately 10^{-5} Torr
	Rate of vapor deposition	$10 \sim 500 \text{ \AA/min}$
	Vapor source	Tantalum chimney board
	Substrate temperature	Room temperature
	Substrate material	Disk, plastic plate, and glass plate

The optical and physical properties of these pigments are subject to change according to the particular coordination metal (M), the chemical structures of substitution groups X and Xm, and the type of crystalline system employed.

a) Coordination metal

Either a bivalent or trivalent metal atom can be introduced as central metal M. As show in Table 3 and Figures 4 and 5, compared with the phthalocyanine pigment, due to the expansion of conjugate π electrons, this substance undergoes a shift in its absorption peak to a longer wavelength, and shows decreases in its thermal properties such as melting point.

Table 3. Spectral and Recording Characteristics of Naphthophthalocyanine as a Function of Its Central Metal (M)

Compound	Film formation ability (vapor deposition)	Thermal decomposition temperature	Spectral properties		Recording properties	Durability	
			λ_{max}	$R_{(S30)}$		Play-back deterioration	Humidity tolerance
Co-phthalocyanine	⊙	426°C	610	26.0	x	-	⊙
Al-phthalocyanine	⊙	543°C	720	12.0	x	-	o
Hg-naphthophthalocyanine	⊙	540°C	720	8.0	Δ	o	⊙
Co-naphthophthalocyanine	⊙	385°C	660	28.4	x	-	⊙
Xl-naphthophthalocyanine	⊙	450°C	700	5.8	x-Δ	-	⊙
Ti-naphthophthalocyanine	o	433°C	840	13.4	Δ-o	o	Δ
Al-naphthophthalocyanine	⊙	483°C	825 ~	27.3 ~	o	⊙	⊙

Reflectivity: R:5 mirror reflection

Playback deterioration: evaluated on disks

$L/V = 6 \text{ m/s}$ $P_a = 0.7 \text{ mW}$

Environmental tolerance: 60°C x 90% RH x 3000 Hrs

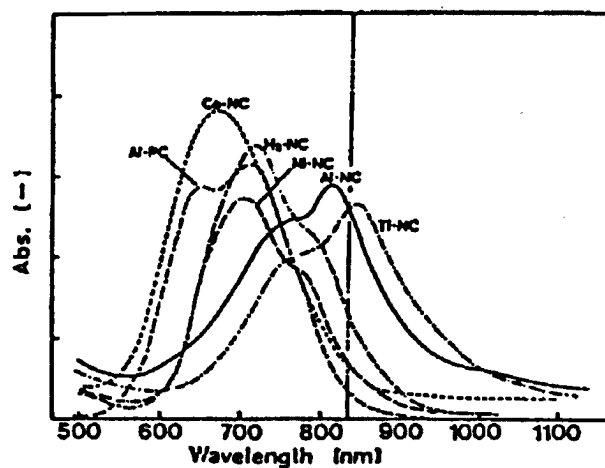


Figure 4. Central Metal and Spectral Properties

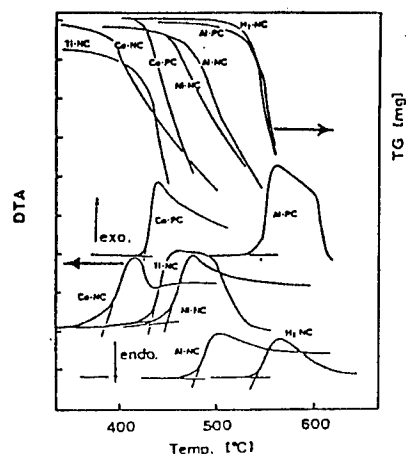


Figure 5. Thermal Analysis Data

Introduction of a metal atom also improves the crystalline stability of the substance. Although the use of V, Sn, and Si as central metals has previously been reported, our experiments indicated that aluminum and titanium metals are particularly effective in improving the optical recording properties of the substance relative to LD laser recording.

As mentioned above, different synthetic and after-treatment methods employed different crystalline types (stable β -type and unstable α -type). In vacuum vapor deposition, the stable type was easier to use for film formation and offered better recording medium properties.

b) Substitution groups (X, X_m)

The aforementioned substitution groups were introduced into X and X_m. Depending on the particular type of solution used, the kind of group introduced became very important. In film formation by vapor deposition, there have been reports on the introduction of a fluorine atom.¹⁰

Table 4. Spectral and Recording Characteristics Relative to the Cl Content of Al-Naphthophthalocyanine

Sample	Cl content (per-cent)	Vapor deposition ability	Thermal decomposition onset temperature	Spectral properties λ_{max}	$R_{(S30)}$ (per-cent)	Recording characteristics	Durability Playback deterioration	Humidity Tolerance
AlNc								
-1	0	Δ	463°C	810	22.0	o	o	x- Δ
-2	2.1	\odot	483°C	825	27.3	o	\odot	o
-3	4.0	\odot	485°C	845	27.6	o	\odot	o
-4	14.9	o	484°C	820	25.1	o	\odot	Δ -o
-5	22.2 %	x- Δ	485°C	820	26.5	Δ	\odot	Δ

Reflectivity: R:5 mirror deflection

Playback deterioration: evaluated on disks

LV = 6 m/s Pa = 0.7 mW

Environmental tolerance: 60°C x 90 % 22 x 3000 Hrs

According to the experiment we conducted, as shown in Table 4, chloride Al-Nc with a chlorine atom introduced showed good recording properties. The recording properties varied with the chlorine content. As shown in Figure 7, the powder X-ray diffraction patterns, along with the ability of the substance to undergo vapor deposition, varied according to the Cl content, and as shown in Figure 8, the resulting films showed different optical and thermal properties. A recording film made by vapor deposition of a powder containing approximately 4 percent of Cl, compared with a theoretical maximum of 4.6 percent by weight, showed good recording properties. It appears that this result is attributable to the film state of thin films, to be discussed below.

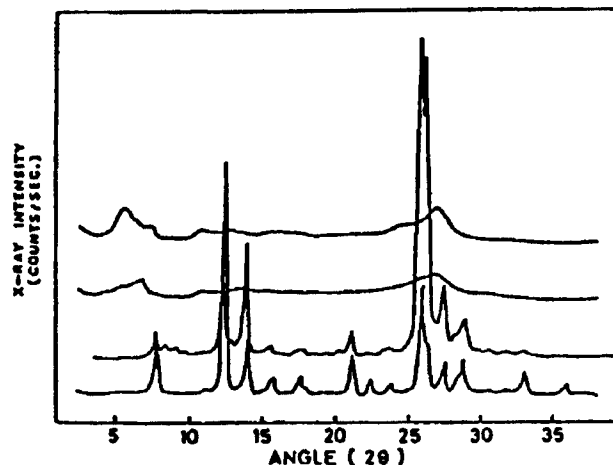


Figure 6. Relationship Between Al-Nc Synthesis and Resulting Crystal Type
--X-ray diffraction graph (powder)

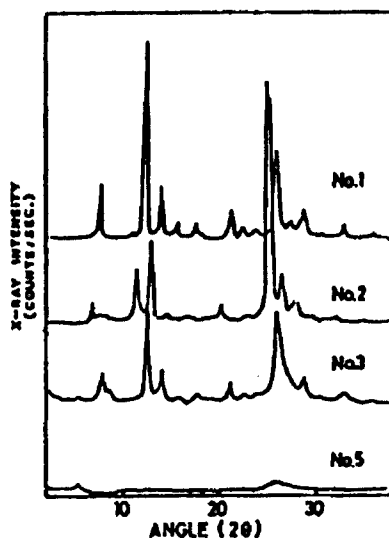


Figure 7. Chlorine/Oxygen Contents and
X-Ray Diffraction Chart (powder)

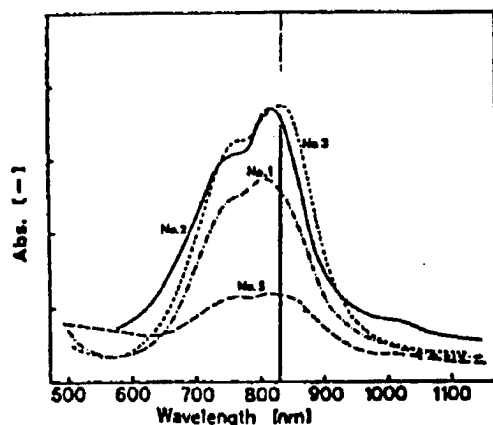


Figure 8. Chlorine/Oxygen Contents and Spectral Properties

5. Relationship Between the Film State (Crystal State) and Recording Characteristics of a Recording Film

The film state (film surface quality, uniformity, crystal state, etc.) of a recording film has significant bearing on its recording characteristics, such as the C/N ratio and optical characteristics (Table 5).

Vacuum vapor deposition for film making involves condensation of organic molecule vapor on the substrate; therefore, the quality of film made by this process is determined by the interactions of the vapor deposition conditions (temperature, rate of reaction, degree of vacuum, etc.). The mechanism of formation of films by organic molecule vapor deposition has been a subject of treatment in a number of publications.^{11,12,13}

Two-dimensionally spread ring molecules, such as naphthophthalocyanine and other multi-ring aromatic compounds, get stacked parallel to the molecule plane due to intermolecular π -electron interactions, and, as shown in Figure 9,¹³ are said to achieve planar molecular orientation growth. It has also been reported that such an orientation state also assumes an internal atomic array, as shown in Figure 9(a) and (b), due to the prevailing substrate surface state and to interaction between pigments.

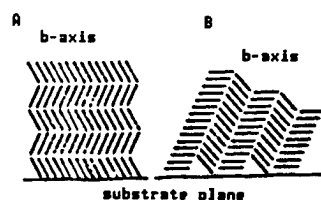


Figure 9. Oriented Growth of Planar Molecules

Table 5. Relationship Between Vapor Deposition Conditions and Film State

Media characteristics	Film state	Vapor deposition factors
		<ul style="list-style-type: none"> Rate of vapor deposition Vapor deposition mode (shutter open/closed, preliminary heating start time, etc.) Chimney temperature (voltage control)
Spectral properties	Uniformity	<ul style="list-style-type: none"> Degree of vacuum (degree of vacuum during vapor deposition, residual gas) Pigment purity (impurities, purification process, crystal type)
Recording properties	Crystal state	<ul style="list-style-type: none"> Pigment physical properties (melting point, sublimation temperature) Substrate (thermal conductivity, surface conditions, type)
Durability	Surface	<ul style="list-style-type: none"> Substrate temperature (radiation heat, heating temperature) Type of vapor source (chimney board geometries) Vapor source-substrate distance Other (substrate rotation, sample volume)

The vapor-deposited film of chloride-Al-naphthophthalocyanine which we prepared has the type of vapor deposition stratified layer shown in the FE-SEM image of Figure 10 (Hitachi, Ltd., S-900). Thin film X-ray diffraction analysis of this film indicates that the film is noncrystalline, as shown in Figure 11. Electron beam diffraction patterns obtained on this sample indicate that the film is disoriented, as shown in Figure 12 (a),(b). As stated above, the quality of the film can be controlled by selecting appropriate vapor deposition conditions. Table 6 presents the results of exerting crystal controls on the film, as reflected in the resulting media properties.



Figure 10. Cross-Section of a Vapor-Deposited Film

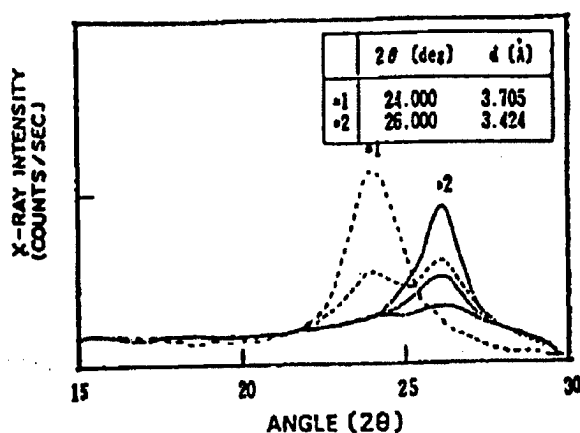


Figure 11. Crystalline Structure of Al-Nc Vapor Deposition Film and X-Ray Diffraction Chart

The results indicate that a recording medium containing large numbers of noncrystalline constituents is superior to a crystal-oriented recording film in noise and recording sensitivity. Thin film thermal analysis (DSC) measurements on this film indicate the presence of a transition point in the neighborhood of 250°C, as shown in Figure 13. Also, it has been determined that the film has a high value of d when subjected to the type of X-ray diffraction analysis shown in Figure 11. These facts would seem to suggest that the change in the axis of orientation shown in Figure 9 might be attributable to a change in the microstructure of the film.

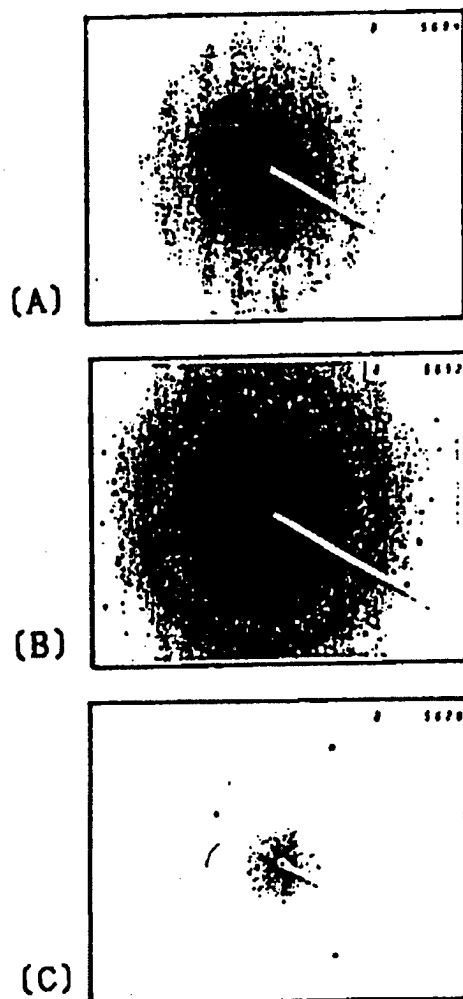


Figure 12. Electron Beam Diffraction Images

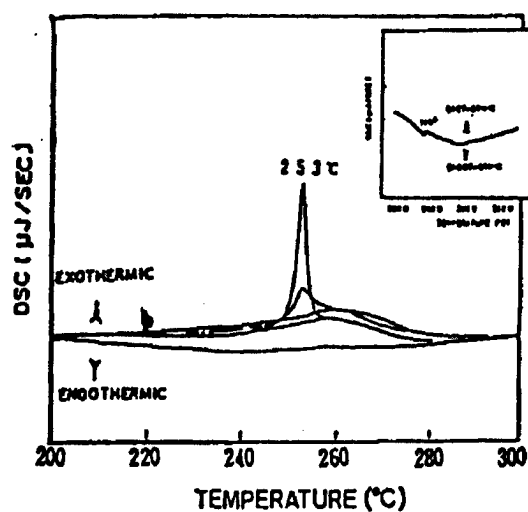


Figure 13. Crystalline Structure and Thermal Properties of Al-Nc Vapor Deposition Film

There have been some reports on film states of (naphtho)phthalocyanine vapor deposition films.¹⁴⁻¹⁸

Table 6. Chloride Al Naphthophthalocyanine Film States and Media Characteristics

Sample name	Observed film states				Media characteristics		
	X-ray diffraction Percent of non-crystalline material $\left(\frac{C-A}{C}\right)$	Thermal analysis (crystallinity)	Spectral properties		Recording characteristics	Durability	
			λ max	R (830)		Playback deterioration	Humidity tolerance
C	0.0	-	750 ^{nm}	12.3	x	-	$\Delta \sim O$
A-1	10.3	High	825	18.4	$\Delta \sim O$	O	O
A-2	55.6		825	26.2	O	⊙	O
A-3	67.1		825	27.0	O	⊙	O
A-4	93.7	Low	825	30.1	O	$\Delta \sim O$	$\Delta \sim O$
Remarks	C: 100% crystalline (300°C heat treated temperature)		Reflectivity R: 5% Mirror reflection			Evaluated on disks LV = 6μ/s P _h = 0.7mW	60°C x 90% RH x 3000 hrs

6. Media Characteristics of a Naphthophthalocyanine Vapor Deposition Film

a) Optical properties

In terms of spectral properties, recording film consisting of an Nc vapor deposition film produces a maximum value matching that of semiconductor lasers, as shown in Figure 14, and produces the film of high reflectivity necessary for data recording and playback. The optical properties of this film are shown in Figure 15. The maximum value of the reflecting curve relative to film thickness corresponded to a high C/N value in a film with 800-900 Å thickness.

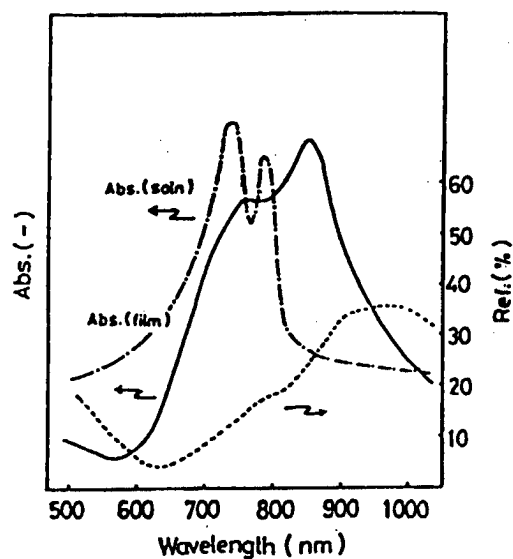


Figure 14. Spectral Properties of a Vapor-Deposited Medium

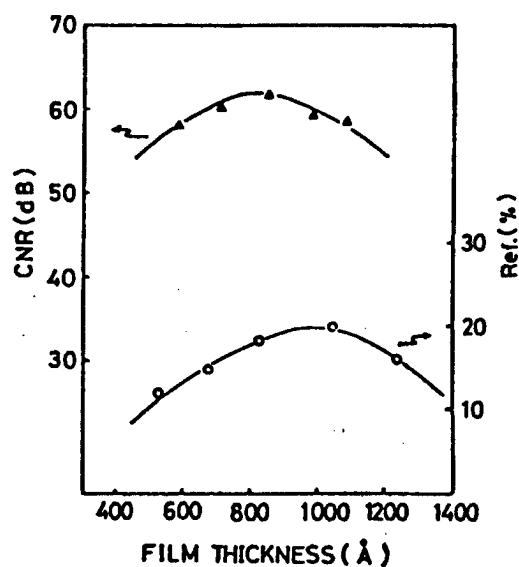


Figure 15. Film Thickness and Recording Characteristics of a Vapor-Deposited Medium

b) Recording characteristics

Figure 16 shows a cross sectional SEM image of pits actually written on the recording film. The recording/playback characteristics ($P_w \times C/N, \text{MHz} \times C/N$) of the recording film are shown in Figures 17 and 18.

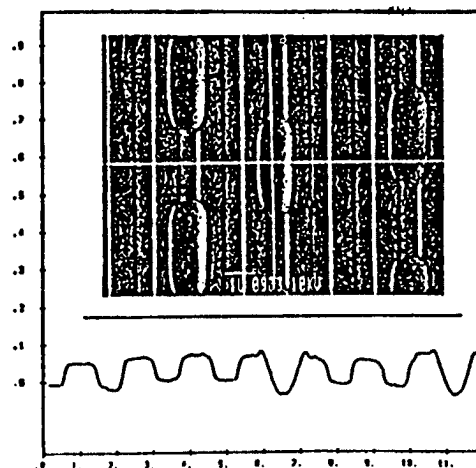


Figure 16. SEM Image of Pits

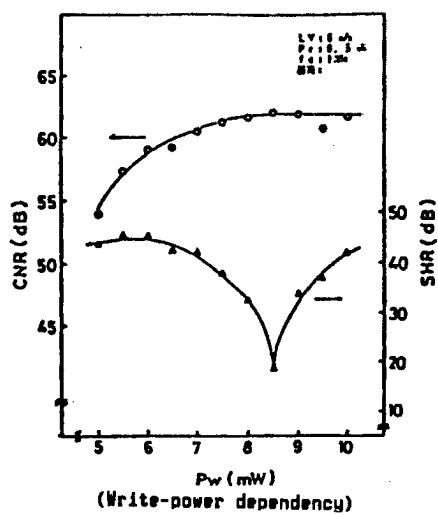


Figure 17. Characteristics of a Vapor-Deposited Disk

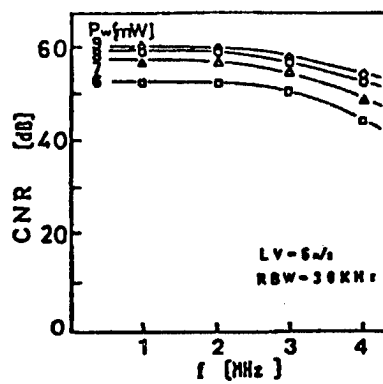


Figure 18. Recording Frequency and Recording Characteristics

c) Durability

Compared with recording films made of polymethylene cyan pigments, which can be used only with a playback beam output of 0.5 mW or less, recording films made of Nc offer a durability which is equal or even superior to metals, relative to playback beam intensity (Figure 19). As would be expected from the fact that NC is used in cosmetic products, films made of this compound offer excellent environmental tolerance, as shown in Figure 20.

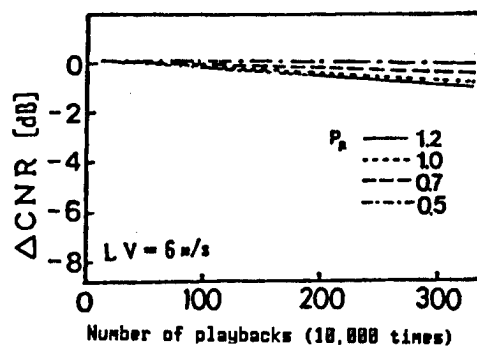


Figure 19. Playback Deterioration
(Number of playbacks (10,000 times))

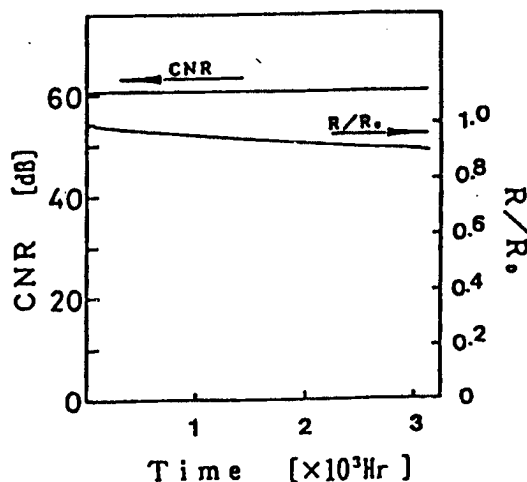


Figure 20. Environmental Tolerance (60°C x 90 percent RH)

References

1. FUTURE ELECTRONICS, MR 1, 1986, p 117.
2. IEE JOURNAL OF QUANTUM ELECTRONICS.
3. USP. No 3475760.

4. THIN SOLID FILMS, Vol 87, 1982, p 215.
5. PHILIPS TECH. REV., Vol 41, 1982, p 325.
6. J. VAC. SCI. TECHNOL., Vol 18, No 1, 1981, p 105.
7. J. APPL. PHYS., Vol 61, No 1, 1987, p 74.
8. OPTICAL RECORDING TECHNOLOGY AND MATERIALS, CMS, 1985, p 189.
9. The 1986 Riken Institute Symposium, 14.
10. The 50th Spring Meeting of the Japan Chemical Society, 1985.
11. J. CHEM. PHYS., Vol 69, 1978, p 3940.
12. SURFACE, Vol 24, 1986, p 61.
13. Ibid., Vol 25, 1987, p 11.
14. J. CHEM. SOC. FARADAY TRNS., Vol 1, No 78, 1985, pp 2773-2785.
15. PHYS. STAT. SOC. (a), 60, 1980, K17.
16. BULL. CHEM. SOC. JPN., Vol 39, 1966, p 2625.
17. ACTA. CRYST., A37, 1981, pp 692-697.
18. Ibid., B40, 1984, pp 263-271.

20138/9365

Preparation of Polyethylene Thin Film Using ICB Method

43063801e Wako-shi BUNSHISEI CHOHAKUMAKU in Japanese Jan 88 pp 39-48

[Article by Horiaki Usui, Ion Engineering Experimental Facility, Faculty of Engineering, Kyoto University]

[Text] 1. Introduction

Recent syntheses of organic molecules having a number of performance characteristics such as conductivity and photosensitivity have stirred interest in their possible applications as novel electronic devices. An advantage of organic materials is that they lend themselves to varied molecular design through a combination of functional groups and molecular structures. Furthermore, unlike an inorganic semiconductor which functions as a crystal, an organic material can permit its constituent molecules to realize independent functions, offering the potential of incorporating a high degree of versatility at a high device density. Essential to the development of new functional devices using an organic material is an organic film formation technology for controlling molecular orientation, morphology, and surface properties. An important challenge facing current semiconductor technology is wider use of dry processes. For the development of new devices using such existing technology, the ability to form organic thin films in a vacuum would be very welcome. Although vacuum vapor deposition has been used widely as a means of creating thin films in a vacuum, the increasing complexity of devices has demanded high-quality films, and existing techniques have proven increasingly inadequate in forming films with a sufficient degree of freedom. Thus, the "ion engineering method" for controlling thin film formation through the use of ions has been proposed.^{1,2} As part of this direction of research, the author has been conducting research on the application of the ion cluster beam (ICB) method to fabrication of organic thin films.

Due to kinetic energy and electrical charge effects, the use of ions can produce films with a number of useful features.^{3,4} The kinetic energy inherent in ions can perform the following functions: 1) cleaning the substrate and film surface and intermediate layer formation by sputtering; 2) intermediate layer formation by ion injection; 3) localized heating of the deposited surface; 4) promotion of condensed nucleus formation; and 5) migration effect, i.e., substrate surface diffusion of deposited particles. To enhance these effects, ionic kinetic energy must be

maintained within the range of a few eV to a hundred eV per molecule--in particular, under 100 eV. On the other hand ionic electrical charges also: 1) promote nucleus formation, nucleus growth, and crystalline growth; and 2) help invigorate quantities of ions present in the vaporized particles. However, since such low-energy ion beams have a large space electrical charge effect, they are not easy to generate in transport in a high vacuum with an adequate degree of control. To address this problem, the ICB method uses ion clusters, an aggregation of loosely coupled molecules, to generate a high-capacity ion beam which is low in equivalent energy. An added advantage of using clusters is the promotion of migrations.

The ICB method has been used successfully in the preparation of numerous inorganic thin films. In the area of organic materials, the technique has been tried for vapor deposition of anthracene,^{5,6} copper phthalocyanine,^{7,8} methylnitroaniline,⁹ and polyethylene.^{6,10,11} Among these, polyethylene is a polymer material of fundamental importance and is well known as an excellent electrical insulator. Therefore, this paper will report on the crystallinity, electrical properties, and chemical purity of polyethylene thin films made by the ICB method.

2. Preparation of Polyethylene Thin Film by the ICB Method

Figure 1 shows the structure of typical ICB vapor deposition equipment. Although details of its operating principles may be found elsewhere,¹² in a nutshell the equipment works as follows. A vapor deposition material is put in a crucible, vaporized, and injected into a high vacuum through a nozzle. In this process, if the mean free path of the vapor inside the crucible is enough smaller than the nozzle diameter, the injected vapor becomes an ultrasonic nozzle stream and is supercooled by adiabatic expansion. The ensuing condensation phenomenon produces clusters. The resulting clusters, partially ionized by an electron beam and accelerated by an electric field, end up forming a thin film on the substrate.

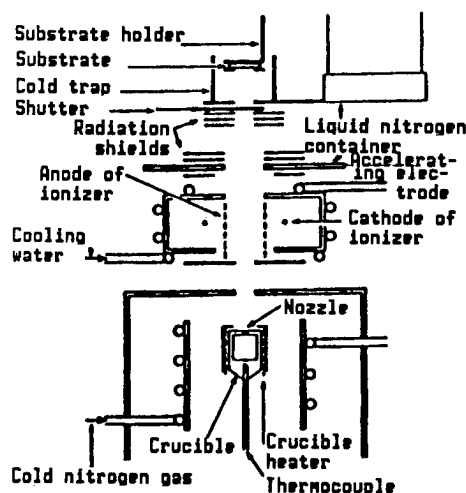


Figure 1. Structural Diagram of ICB Vapor Deposition Equipment

Experimental and theoretical investigations of the process of cluster formation are being conducted using anthracene. From analyses of cluster beam velocity, it has been confirmed that the injected vapor forms an ultrasonic nozzle stream, and that it is cooled by adiabatic expansion.¹³ Also, from analyses of ion cluster beam energy it has been demonstrated that a cluster consists of about 10 molecules. Furthermore, the mechanism of cluster formation can be explained using the classical theory of condensation. Based on this fact, computer simulation studies of the process of cluster formation have been carried out.¹⁴

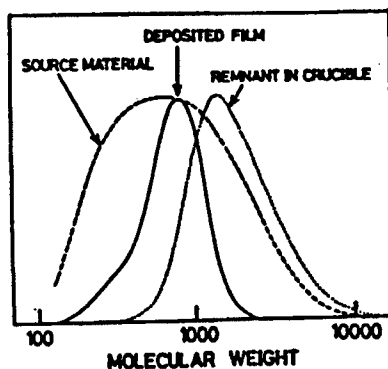
For vapor deposition of polyethylene, as the raw material we used polyethylene powder. Specifically, for most purposes we used Hi-wax100p (viscometric mean molecular weight $M_v = 900$, density = 0.95) and Hi-wax400p (viscometric mean molecular weight $M_v = 4000$, density = 0.97), both made by Mitsui Petrochemical Industries, Ltd. The crucible was heated gradually, over a period of an hour or more, in order to thoroughly degas the vapor deposition material. At a crucible temperature of 310-330°C, a vapor deposition rate of 4-8 nm/min was achieved. For ionization, an electron current I_e of 10-20 mA was used. The voltage of acceleration, V_e , of ionizing electrons was held at 50 V. Ion acceleration voltage V_a is an important parameter bearing heavily on the quality of the resulting film; this parameter was allowed to vary within the 0-2000 V range. The degree of vacuum used during vapor deposition was 5×10^{-6} torr.

As substrates, we used silicon wafers, Corning 7059 glass, and sodium chloride. Glass substrates were washed ultrasonically with trichloroethylene and acetone, and were heat-treated for 1 hour at 120°C in a vacuum prior to vapor deposition. Silicon substrates were given the same pretreatment, except that in the case of these substrates organic solvent washing was followed by hydrofluoric acid treatment to remove the naturally formed oxide films. The NaCl substrate was cleaved in air and used without any pretreatment. In most cases, during vapor deposition the substrate temperature was held at room temperature.

3. Molecular Weight Distribution and IR Absorption Characteristics

As a rule, polymers are difficult to gasify, and are liable to molecular decomposition when heated. In view of this fact, the molecular weight distribution in the deposited films was measured by means of gel permeation chromatography (GPC). Figure 2 shows molecular weight distributions in the raw material, deposited film (without ionization), and the residues in the crucible after vapor deposition, for both Hi-wax100p (a) and Hi-wax400p (b). In the former, the mean molecular weight of the deposited film was not significantly different from the molecular weight of the raw material; however, in the latter the molecular weight of the deposited film was substantially lower, indicating that in materials containing heavy molecules, vaporization causes breakage of molecular chains. However, each case showed a highly uniform molecular weight distribution, indicating that the ICB method affords an effective means of controlling film qualities such as crystallinity.

(a) Hi-wax100p



(b) Hi-wax400p

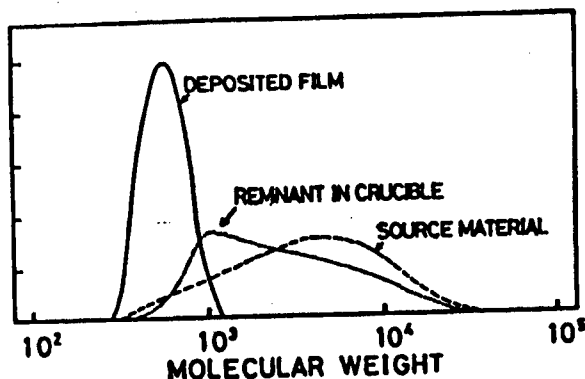


Figure 2. Molecular Weight Distributions in the Raw Materials, Deposited Films, and Crucible Residues for (a) Hi-wax100p and (b) Hi-wax400p

Figure 3 shows the IR absorption characteristics of raw material Hi-wax100p and those of deposited films. The IR absorption characteristics of deposited films agreed with those of ordinary crystalline polyethylene, and no absorptions that might be attributed to an impure molecular structure or amorphous structure were observed. The deposited films showed a somewhat lower absorption by the methyl group, compared with absorption patterns of the raw material. It appears that decreased absorption is due to breakage of side chains during vaporization, causing the molecules to be deposited as linear molecules, and should contribute to improvements in film density and crystallinity.

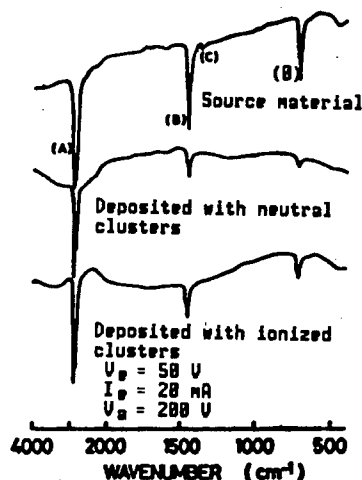


Figure 3. Infrared Absorption Characteristics of Hi-wax100p Raw Material and Deposited Films

4. Crystallographic Properties

Ordinarily polyethylene crystallizes at a rate of 70-90 percent. Polyethylene monocrystals can be obtained only in small fragments after many hours of precipitation for a solution. By contrast, since the ICB method, due to its ionic kinetic energy or electrical charge effects, is capable of controlling the mechanism of film formation or the crystal growth process, and is capable of producing crystals of uniform molecular weight, potentially it affords a means of improving crystallinity.

Figure 4 [not reproduced] shows electron beam diffraction images of Hi-wax100p deposited film made on a silicon substrate (111) by varying the ionization electron current I_e and the ion acceleration voltage V_a . The substrate temperature was maintained at 70°C. Ionization and acceleration of the cluster beam resulted in improved crystalline orientation and produced monocrystalline spot patterns. In this case if we assume side (001) to be parallel to the substrate, on the deposited film the molecular chains are oriented perpendicular to the substrate surface. According to polarization microscope observations, the size of the crystalline particles was about 10 μm each.

The crystallinity of a film is also influenced to a large extent by the condition of the substrate surface. Figure 5 [not reproduced] shows electron beam diffraction images of Hi-wax400p vapor deposition film created on an NaCl (100) substrate which was cleaved in atmosphere. The substrate was maintained at room temperature. In Figure 5(a), in which the substrate was not heat-treated before deposition, films made by depositing clusters without ionization showed ring patterns, indicating random crystalline orientation, whereas films made by ionizing and accelerating clusters showed monocrystal-like spot patterns. By contrast, in Figure 5(b) wherein the substrate was heat-treated before deposition, fiber-like films having some degree of orientation were obtained even if the clusters were deposited without ionization. These results indicate that the kinetic energy of ions can bring about cleaning of the substrate surface.

5. Electrical Properties

Although polyethylene is known to be an excellent electrical insulator, its properties are subject to variation due to the packing density, molecular structure, purity, and shape. The following discusses the dielectric properties, voltage-current characteristics, and insulation voltage tolerance of Hi-wax400p deposited films made by the ICB method. In all cases, the substrate temperature during deposition was maintained at room temperature.

Figure 6 shows the low-frequency dielectric characteristics of an Au-polyethylene-Au sandwiched cell. In this frequency range the dielectric constant of the substance was fixed, and was equivalent to the bulk dielectric constant 2.3. On the other hand, dielectric loss $\tan \delta$ was less than 1×10^{-3} at 5 kHz and higher, and was less than the measurable limit of the bridge used for measurement. As shown in Figure 7, the dielectric constant remained unchanged over a room temperature--100°C temperature

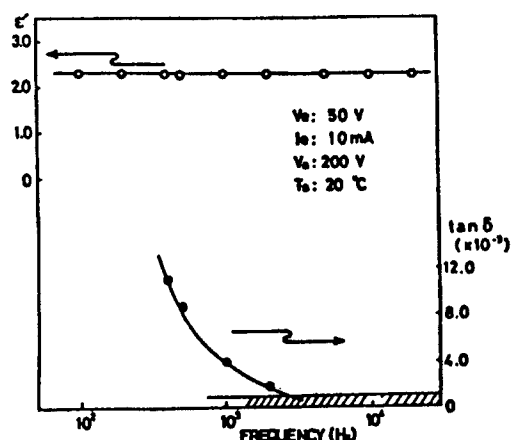


Figure 6. Dielectric Properties of Polyethylene Film

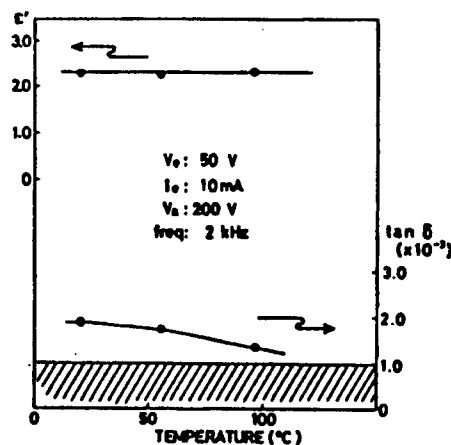


Figure 7. Temperature Dependency of Dielectric Constant of Polyethylene Film

range. These results indicate that films deposited by the ICB method are physically dense and are free of polar impurities.

Figure 8 shows the voltage-current characteristics of a polyethylene thin film 130 nm thick produced on a silicon substrate by changing the deposition conditions. This film, produced under conditions that would normally produce good crystallinity, i.e., $I_e = 10$ mA, $V_a = 1$ kV, or $I_e = 20$ mA, $V_a = 500$ V, showed an ohmic voltage-current characteristic in the low electric field region, and in the high electric field region it showed what appeared to be the typical voltage-current characteristic due to Schottky emission. By contrast, when clusters were not ionized or when an insufficient ion acceleration voltage was used, such ideal characteristics were not obtained. In the ohmic region, the film had a resistivity of 10^{15} to 10^{16} Ωcm .

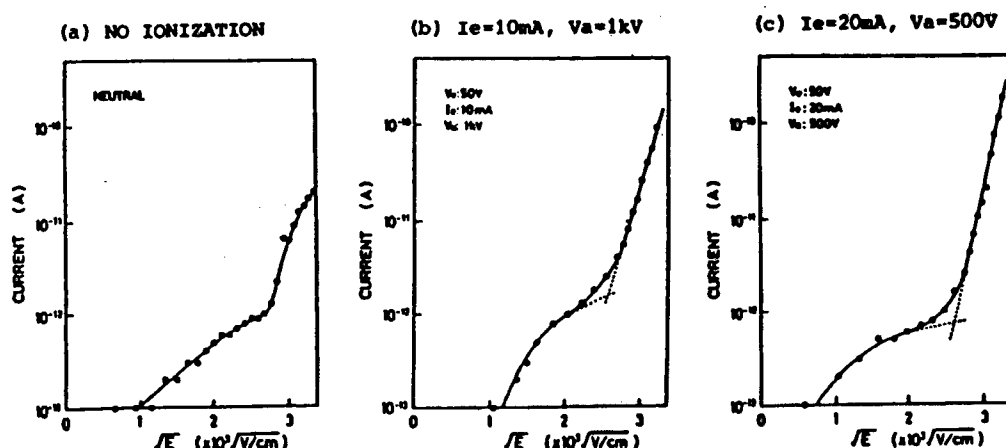


Figure 8. Representative Voltage-Current Characteristics of Polyethylene Film

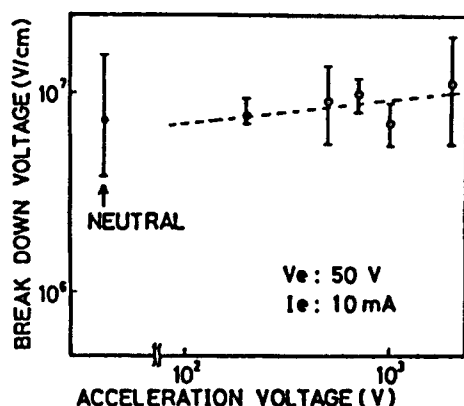


Figure 9. Insulation Breakdown Strength of Polyethylene Film

Figure 9 shows the insulation breakdown strength of a film made on a silicon substrate at $I_e = 10$ mA and made by varying the ion acceleration voltage. With increases in the ion acceleration voltage, the insulation breakdown strength increased somewhat, and a high value of 1×10^7 V/cm with a high degree of reproducibility was obtained even with films 130 nm in thickness.

6. Surface Properties

The film-substrate surface properties are of considerable importance if organic thin films are to find applications in electronic devices. In view of this fact, we evaluated the surface properties of polyethylene thin film-Si substrate interface in terms of the high-frequency capacitance-voltage (C-V) characteristics of an Au-polyethylene-p-Si (100) MIS diode. Figure 10 shows the C-V characteristics at 1 Mhz of (a) cells fabricated without ionization, and (b) cells fabricated with ionization and acceleration. The latter cells exhibit a large capacitance change, with a

diminished flatband shift, indicating improved surface characteristics. The surface level density obtained from the data shown in Figure 10(b) and by using Terman's method was approximately $1.3 \times 10^{11}/\text{cm}^2 \text{ eV}$ near the center of a band gap.

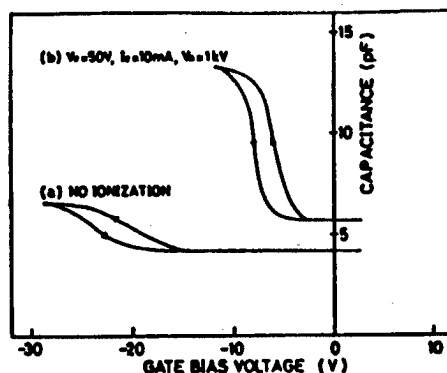


Figure 10. High-Frequency C-V Characteristics of MIS Diode

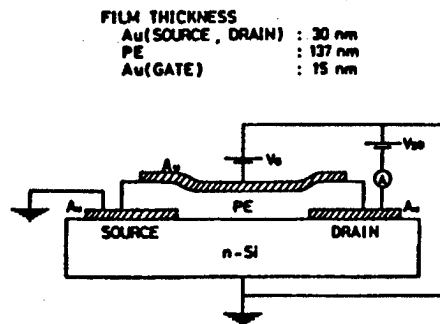


Figure 11. Structural Diagram of MISFET

To study what effect the ability of the ICB method to control surface properties had on device characteristics, we made an experimental version of a MISFET, using polyethylene gate insulation film, on an n-type Si (111) substrate. Figure 11 shows the structure of this device. The source and drain electrodes were made by forming Schottky junction between Au and n-Si. Figure 12 shows representative operating characteristics of (a) a cell for which the polyethylene gate insulation film was prepared without ionization, and (b) a cell prepared under $I_e = 10 \text{ mA}$ and $V_a = 1 \text{ kV}$ conditions. In these data the leak current at Schottky junctions has been subtracted. Cell (b) produces substantially higher source-drain current than cell (a), and shows typical output saturation, indicating the formation of an inverted layer. With a gate voltage of 30 V or higher, the square root of source-drain saturation current increases proportionally with the gate voltage. Although this device could use improvements in cell

structure and other areas, it demonstrated that use of the ICB method can improve film-substrate surface properties, with corresponding improvements in device properties.

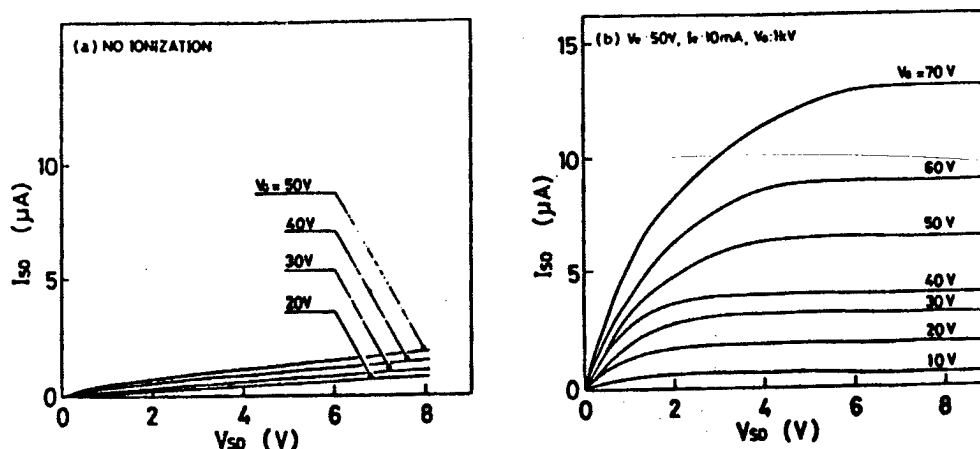


Figure 12. Output Characteristics of MISFET Prepared
(a) Without Ionization, and
(b) With Ionization and Acceleration

7. Analyses by Second-Order Ion Mass Spectrometer (SIMS) and X-Ray Electron Spectroscopy (XPS)

It is possible that the excellent electrical properties of the ICB-deposited polyethylene films discussed in the foregoing are related to the high degree of chemical purity of the films. In plasma-polymerized films, for example, residual radicals of impure molecular structures present in the film can contribute to dielectric loss or film stability problems. Therefore, to identify the characteristics of ICB-deposited films, we have conducted SIMS and XPS analyses.^{15,16} For comparison, plasma-polymerized ethylene (PPE) films were also analyzed. The PPE film was prepared by parallel plate glow discharges on ethylene monomer gas. When monomer gas was introduced at a flow rate of 10 sc cm into a chamber vacuumed up to 1×10^{-6} torr until a pressure of 1×10^{-2} torr was reached, and when glow discharges were conducted at 20 kHz and 100 mA, film was formed at the rate of 5 nm/min.

SIMS analysis was conducted under 3 keV, 0.6 μ A argon ion sputtering by an Anelba SIMS-300N machine. Figure 13 shows secondary negative ion spectra of ICB and PPE films, measured immediately after argon ion irradiation, and 15 minutes and 13 minutes afterward, respectively. The main secondary negative ion species found were H, C, CH, O, OH, C₂, and C₂H. Figure 14 shows the C- secondary ionic strength as a function of argon ion irradiation time. Immediately after the argon ion irradiation, secondary ion discharges from the ICB film of any of the above ionic species were low; with increases in ion irradiation time, the discharges gradually increased, eventually reaching a constant value. By contrast, the PPE film started showing a high rate of secondary ion discharge immediately after the beginning of ion irradiation.

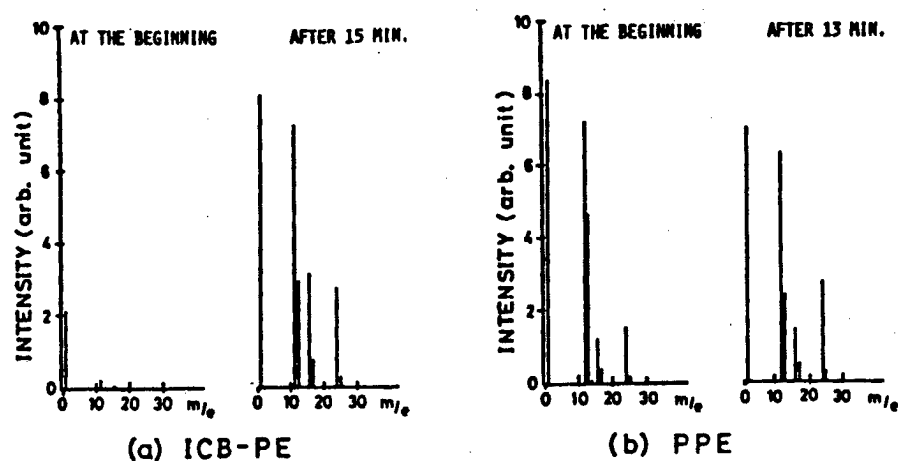


Figure 13. Secondary Negative Ion Spectra of ICB Film (a) and PPE Film (b)

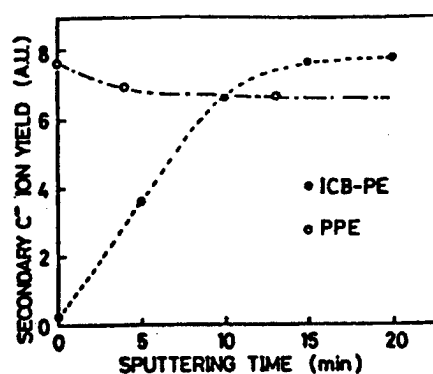


Figure 14. Time-Dependent Change in C- Discharge Rate

The XPS analyses were conducted by using a Shimazu ESCA-750, along with argon ion beam sputtering at $500 \text{ eV} \cdot 10 \mu\text{A}$ as necessary. Figure 15 shows XPS peak spectra of C_{1s} and O_{1s} of ICB and PPE films for different argon sputtering times. From these data, it is evident that ICB-deposited films contain much less oxygen than PPE films. The O_{1s} signal strength of ICB films is close to the detectable limit; such a quantity is always observed at the surface of ordinary materials. Table 1 shows the O_{1s}/C_{1s} signal strength ratios of ICB and PPE films prepared with different ion acceleration voltages. For comparison purposes, measurements of typical high-density and low-density polyethylene films are also shown. Compared with either type of polyethylene film, the ICB film has a low oxygen content. Furthermore, it is apparent that application of ion acceleration reduced the amount of oxygen in the film. Although the oxygen content of ICB films initially increases due to the action of argon ion sputtering and falls subsequently, at any rate the magnitude of change is small. On the

other hand, the PPE film seems to lose a great deal of oxygen due to ion sputtering. Also, although the C_{1s} spectrum of ICB films has a symmetric shape, with a half-value width of 1.55 eV, the value increases to 1.80 eV after 30 minutes of sputtering. By contrast, the C_{1s} spectrum of PPE films is nonsymmetric, with a higher, 1.95 eV, half-value width; but this value decreases to 1.80 eV after 30 minutes of argon sputtering.

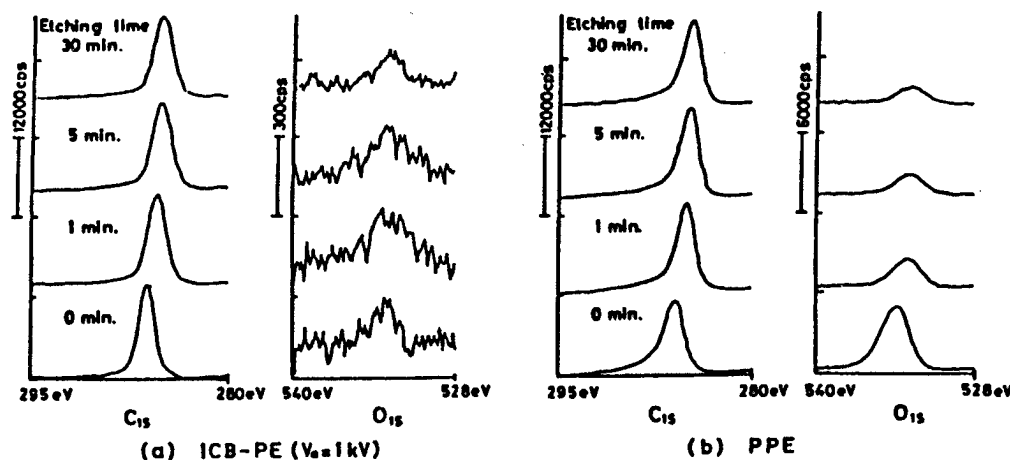


Figure 15. XPS Spectra of ICB Film (a) and PPE Film (b)

Table 1. O_{1s}/C_{1s} XPS Signal Strength Ratios of Various Polyethylene Films

Etching time (minutes)	ICB - PE* ¹			PPE* ²	HDP* ³	LDP* ⁴
	Neutral	$V_a=200$ V	$V_a=1$ kV			
0	0.014	0.009	0.008	0.17	0.15	0.14
1	0.017	0.009	0.020	0.071	0.11	0.078
5	0.015	0.013	0.012	0.050	0.096	0.036
30	0.015	0.011	0.007	0.045	0.080	0.0207

The following may explain the above results of SIMS and XPS analyses. Because of the presence of many impure molecular structures chemically adsorbed in the film or especially on the film surface due to the effects of residual radicals, the PPE film has high oxygen content; the film is also chemically unstable, which may account for its high secondary ion discharge rates and large XPS peak half-value widths. On the other hand, the ICB film is chemically stable because of its high degree of film purity and crystallinity, which may account for its low oxygen content and low secondary ion discharge rates. Sputtering the film with an ion beam, with attendant radiation damage, causes lattice defects and destroys molecular structures. These events, in turn, tend to increase the secondary ion discharge rate and broaden the XPS peak half-value width, as with the case of the PPE film.

8. Conclusion

Because of its ionic kinetic energy and electrical charge effects, the ICB method provides a unique means of forming thin films. In this report, we have shown that the ICB method can be employed for the preparation of polyethylene films having a high crystalline orientation and a high degree of purity. Reflecting these characteristics of the method, ICB-deposited films exhibited excellent electrical properties. It has also been shown that use of the ICB method can improve film-substrate surface properties. The above results relating to film formation through the use of ions are also applicable to organic materials, and suggest considerable potential for use in the development of electronic devices.

References

1. Toshinori Takagi, ELECTRONICS, October 1981, p 1091.
2. Ibid., NIKKEI ELECTRONICS, 7 December 1981, p 188.
3. T. Takagi, THIN SOLID FILMS, Vol 92, 1982, p 1.
4. Ibid., J. VAC. SCI. TECHNOL., Vol A2, 1984, p 382.
5. H. Usui, M. Nauemura, I. Yamada, and T. Takagi, Proc. 6th Symp. Ion Sources and Ion-Assisted Technology, Tokyo, 1982, p 331.
6. H. Usui, I. Yamada, and T. Takagi, J. VAC. SCI. TECHNOL., Vol A4, 1986, p 52.
7. H. Usui, M. Nauemura, H. Nakanishi, I. Yamada, and T. Takagi, Proc. 8th Symp. Ion Sources and Ion-Assisted Technology, Tokyo, 1984, p 271.
8. F. Nakanishi, H. Takata, H. Usui, I. Yamada, and T. Takagi, Proc. 9th Symp. Ion Sources and Ion-Assisted Technology, Tokyo, 1985, p 449.
9. H. Dohmoto, H. Usui, I. Yamada, and T. Takagi, Proc. 11th Symp. Ion Sources and Ion-Assisted Technol., Tokyo, 1987, p 451.
10. H. Usui, I. Yamada, and T. Takagi, Proc. Intern. Ion Eng. Cong.-- ISIAT'83 IPAT'83, Kyoto, 1983, p 1247.
11. H. Dohmoto, F. Nakanishi, H. Usui, I. Yamada, and T. Takagi, Proc. Intern. Workshop Ionized Cluster Beam Technique, Tokyo and Kyoto, 1986, p 171.
12. Toshinori Takagi, APPLIED PHYSICS, Vol 55, No 8, p 746.
13. H. Usui, E. Kato, I. Yamada, and T. Takagi, Proc. 8th Symp. Ion Sources and Ion-Assisted Technol., Tokyo, 1984, p 297.

14. H. Usui, I. Yamada, and T. Takagi. Proc. Intern. Workshop Ionized Cluster Beam Technique, Tokyo and Kyoto, 1986, p 63.
15. K. Numata, H. Usui, I. Yamada, and T. Takagi, Proc. ACS National Meeting, Vol 56, Denver, 1987, p 151.
16. K. Numata, H. Usui, I. Yamada, and T. Takagi, Proc. 11th Symp. Ion Sources and Ion-Assisted Technol., Tokyo 1987, p 457.

20138/9365

Preparation of Phthalocyanine Film by OMB Method

43063801f Wako-shi BUNSHISEI CHOHAKUMAKU in Japanese Jan 88 pp 49-54

[Article by Masahiko Hara, Molecular Devices, Riken Institute]

[Text] 1. Introduction

Construction of "molecular devices" requires the development of techniques for placing organic molecules in specific directions or in designed spatial configuration. It is virtually impossible to control the direction of individual molecules in a three-dimensional aggregate of organic molecules. As a more realistic goal, we must explore the possibility of controlling the orientation of organic molecules to form regular patterns in a film, or stacking such films.

At present, the methods for creating films by conferring a certain directionality in a layer, and by stacking the molecules by layers, fall into two broad categories: the wet method, typified by the LB method treated in the preceding pages, and the dry method using a vacuum. Although epitaxially grown films are attractive from the standpoint of creating hybrid layers with inorganic metallic atoms and also from the standpoint of surface compatibility with dissimilar substances, such films cannot be realized by existing methods. In view of this fact, the author and his colleagues have been studying organic molecular beam epitaxy (MBE),¹ normally used on inorganic substances, to organic substances.² In this paper we refer to produced films as "made by the organic molecular beam method," dropping the "epitaxy (E)," for the reason that the technique does not yet allow either confirmation or control of epitaxial growth. Since OMB shares the same methodology as OMBE, the author's ultimate goal is to develop a method that merits an "OMBE" designation.

2. OMBE Method

The underpinnings of the OMBE method are based on the MBE method, and it can be viewed as a type of vapor deposition conducted in an ultravacuum in the 10^{-9} - 10^{-10} torr range. Compared with other vacuum vapor deposition methods, OMBE produces very little residual gas, permits film growth temperature control at low temperature ranges, and offers the potential for formation of highly pure films having exceedingly smooth hetero surfaces. Although ordinarily both OMBE and MBE use crystals having a specific

lattice constant as a vapor deposition substrate, in OMBE the unit cell of organic crystals is substantially larger than the unit cell on an inorganic crystal substrate. For this reason, in OMBE the concept of lattice mismatch that is used in MBE cannot be applied in a simple manner.

Figure 1 shows an OMBE system (machine No 2) currently under development. Although machine No 1 incorporated the ordinary MBE system intended for use in conjunction with organic substances, the new OMBE system offers several features beyond the features available in the conventional MBE systems.

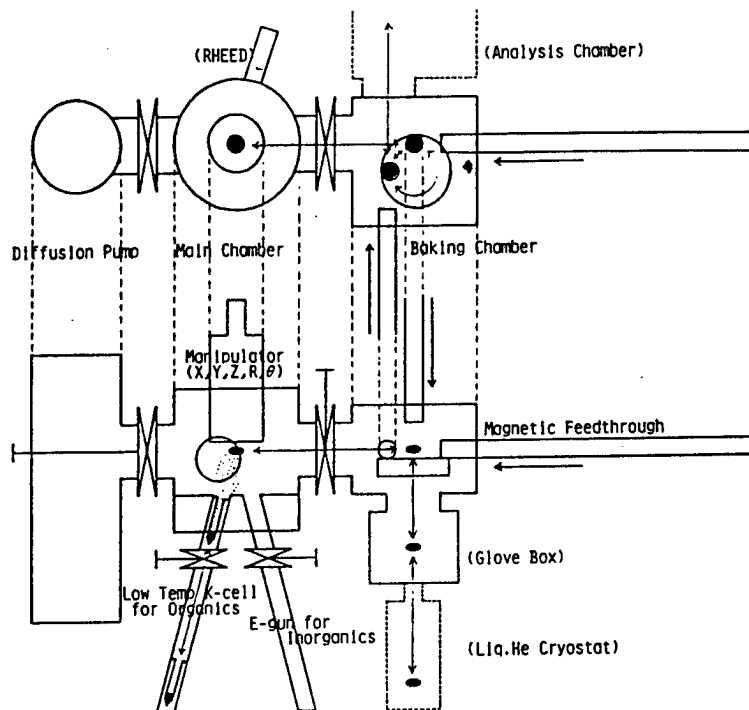


Figure 1. Schematic Diagram of the New OMBE System

As a rule, organic substances have significantly higher vapor pressures than inorganic substances. Therefore, in a supervacuum in the 10^{-10} torr range, most of such substances would sublime even at room temperature. Since most of the commercially available systems control the source of vapor by heating, in such systems the types of organic substances that can be used are necessarily limited. To address this problem, the new OMBE system provides a Knudsen cell capable of controlling the vapor source even under 0°C , and has the ability to keep the substrate sufficiently cooled below the vaporization temperature. The cooling capacity of the system is currently being tested, with a goal of achieving -80°C .

The conventional MBE system carries on baking in the main unit after a sample is introduced. However, if an organic substance was introduced, the sample itself would evaporate, inhibiting sufficient baking. Again, to deal with this problem, the OMBE system is provided with a load/lock

mechanism in the Knudsen cell part, which permits sample replacement in the growth chamber without breaking the vacuum.

3. Organic Film Formation by Dry Methods

In the past, several attempts to create organic films through the use of vacuum vapor deposition have dealt with straight chain molecules, planar molecules, and polymers. However, there have been few cases achieving successful structural control of these films on the substrate, and in particular, those achieving structural control during epitaxial growth have been rare.³ In rare instances, control has been achieved only over a small area or only as a part of a multidomain, on a much smaller scale than the scale of epitaxial growth used in inorganic growth processes.

In fact, at present no method is available for achieving epitaxial growth of organics having a thickness of a few nanometers and an area on the order of 2 to 3 x 100 μm^2 . Although reports on epitaxially grown films have appeared recently, and although epitaxial growth is possible in a partial sense and it is possible to create a continuous film, provided the film has a certain minimum thickness, epitaxial growth in the true sense, i.e., formation of an organic monocrystalline film, has not been achieved.

Research on organic film preparation by dry methods traces back to a study comparing the X-ray diffraction peaks of bulk (powder) and vacuum vapor deposition films undertaken by Inoue, et al., in 1961.⁴ Subsequently, pioneering research on epitaxial growth of organic films was conducted by Somorjai's group during the 1970's.⁵ These efforts constitute the foundation of current OMBE research. These researchers employed the tactic of inducing either vacuum vapor deposition or absorption of multi-ring aromatic compounds on a metal monocrystalline surface, and they attempted to explain the surface structure resulting from the LEED method and the site of epitaxial growth on the basis of the LEED data. Table 1 summarizes their findings.

Most of the other research efforts in regard to epitaxially grown organic molecule films have been concerned with the preparation of substances for observation under high-resolution electron microscopes. Ashida, Ueda, et al., have studied the epitaxial characteristics of phthalocyanine and tetraquinodimethane, which have been vacuum vapor-deposited on a substrate consisting of a cleaved mica surface or an alkali halide monocrystal surface.⁶ More recently, near epitaxial growth has been observed in samples of fatty acid salts covered with germanium to minimize damage due to the electron beam, and through observation of their surface profiles.⁷

In epitaxial growth of organic substances, interaction between molecules as well as interaction between the molecules and the substrate, comes into play. Furthermore, the competition between these types of interactions has a large bearing on the growth pattern. Qualitatively speaking, when the interaction between the molecules and the substrate prevails over the molecule-molecule interaction, the molecules have a higher epitaxial quality relative to the substrate. Especially, for planar molecules having π electron conjugates, among them phthalocyanine, the following mechanism of

Table 1. Structures of Organic Molecules Deposited (Adsorbed) on a Metal Surface

Metal surface	Organic molecule	Surface structure
Pt (100)	Benzene	Amorphous
	Naphthalene	Amorphous
	Pyridine	(1 x 1)
Pt (111)	Benzene	$\begin{vmatrix} -2 & 2 \\ 5 & 6 \end{vmatrix}$
	Naphthalene	(6 x 6)
	Pyridine	(2 x 2)
	Cu-Pc	Amorphous
Ni (111)	Benzene	$(2\sqrt{3} \times 2\sqrt{3})$ R30
Ni (100)	Benzene	C (4 x 4)
Cu (111)	Fe-Pc	Amorphous
	Cu-Pc	Amorphous
Cu (100)	Fe-Pc	$\begin{vmatrix} 5 & -2 \\ 2 & 5 \end{vmatrix}$
	Cu-Pc	
	H ₂ -Pc	

growth has been proposed: the part of the molecule having a high electron density is adsorbed on the positive ion part of the substrate, leading to nucleus generation (Figure 2); subsequently, intermolecular π electron interaction causes column-like stacking of molecules. Such a mechanism of growth suggests that the sites of epitaxial nucleus growth exist randomly on a substrate and are randomly oriented, and the random nature of these sites makes the realization of epitaxial monocrystalline films of organic substances a difficult task.

4. Preparation of Phthalocyanine Film by OMBE

Using the OMBE system, the author and associates have begun to work on the lamination of organic substances including phthalocyanine.⁸ Although normally phthalocyanine has a column structure in which molecules are stacked, it is also known that, depending on the magnitude of interaction between molecules and the substrate, the substance can assume one of the two morphologies shown in Figure 3. The peaks of X-ray diffraction patterns of phthalocyanine film created on glass agree with the interval between the central metal atoms along the film thickness of the phthalocyanine column shown in Figure 3(a). The illustration indicates that since the intermolecular interaction is much stronger than the molecule-substrate interaction, the column axis is parallel to the substrate surface, and consequently the film has a periodicity of layers in the direction of film thickness.⁹ However, it has not been possible to control the molecular orientation within a layer, and in the present state

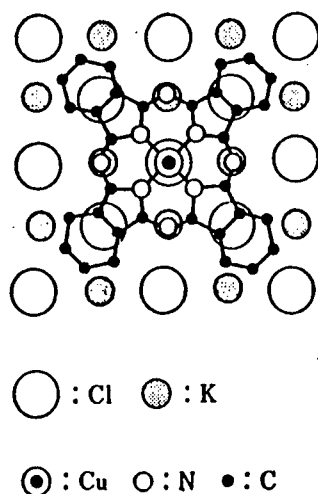


Figure 2. Configuration of Copper Phthalocyanine on KCl

of affairs it is difficult to draw inferences regarding the anisotropy of the film.

It is known that with conventional vacuum vapor deposition the slower the rate of vapor deposition the sharper are the X-ray diffraction peaks. The epitaxial quality of films made by vacuum vapor deposition awaits further research in terms of film-substrate interaction and film formation conditions. One approach might be the generation of a molecular beam in order to use the monocrystals of the substance to be layered as the substrate. However, phthalocyanine monocrystals obtained by sublimation purification are needle-like crystals. Although they can grow to a few millimeters in size, they are highly fragile and consequently cannot be used as a substrate material. Conceivably phthalocyanine films made by the LB method could be used, but such films, when expanded on the water surface, tend to assume island configurations rather than becoming uniform LB film, which would make their use as substrates difficult. This is one of the questions meriting close study.

The author has used the needle probe method (Figure 4) as well as scanning tunnel microscopy (STM) as a way of investigating the film surface condition, an important consideration in attempts to join a given film with another, dissimilar, substance. The results indicate that the OMBE method is capable of forming densely packed film on the order of a few square millimeters in area having extremely smooth surfaces, hitherto not achieved by conventional film growth methods.

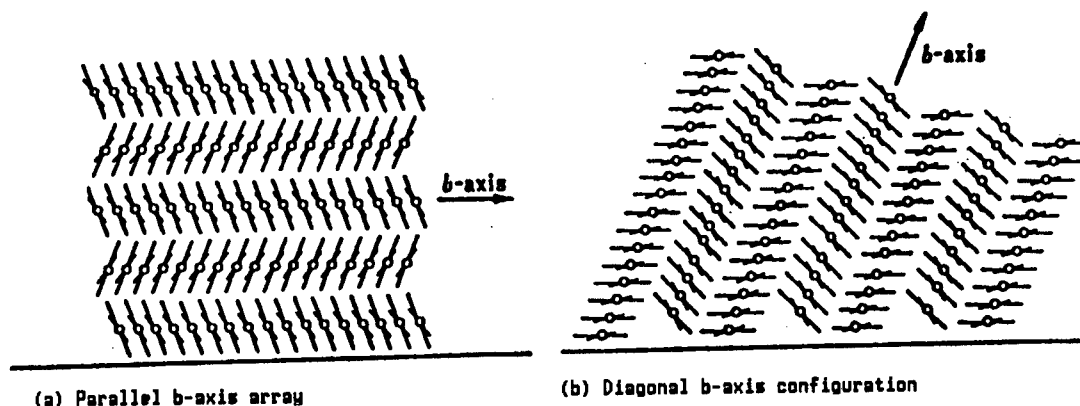


Figure 3. Column Structure and Orientation of Phthalocyanine Crystals

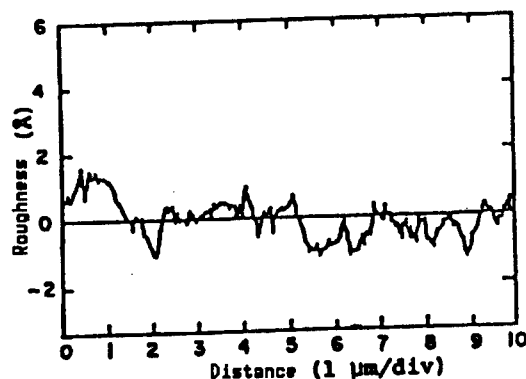


Figure 4. Surface Roughness of Ni-phthalocyanine on Si Wafer, as Determined by the Needle Probe Method

Parts (a), (b), and (c) of Figure 5 [not reproduced] show electron microscope (SEM) pictures of phthalocyanine films made on glass-ITO-silicon (111) surfaces. Photograph (d) [not reproduced] shows a film made by an ordinary vacuum vapor deposition apparatus on a silicon surface. The silicon sample in (c) was photographed by tilting it 30 degrees. It was not until the sample was tilted to this extent that small gradations on the surface became noticeable. In other flat areas, even when the magnification was raised and contaminated parts were focused on, nothing unusual was noticeable, confirming that the surface was exceedingly flat. At present, the relationship between the existence of gradations on the film and the film growth process is not understood. However, when compared with photograph (d), it is evident that the film grown by OMBE has surface patterns quite different from the surface patterns of films grown by conventional means. Furthermore, ITO surfaces used in ordinary electrical properties measurements have a shape wherein the surface is filled with globules about 10 nm in diameter. Growing a phthalocyanine film on top of such a surface would not produce the type of smooth surface shown in these

photographs. At the edge of the globules is the growth of capillary crystals which appear to be phthalocyanine; however, these crystals are so fragile that they disappear (damaged) when electron beam sweeping is applied. Even if a surface, though densely filled, is not smooth, it can yield good Schottky junction interface not possible with conventional organic films.⁹ However, it would be simplistic to assume that a good Schottky quality will translate directly to a good consistency. Good consistency must be realized by epitaxial growth.

According to published data, metal phthalocyanine in bulk form has an electrical conductivity of 10^{-10} to 10^{-14} S/cm, which can be increased by a factor of 10 through iodine doping. By contrast, the phthalocyanine films produced by the methods described in this paper show a conductivity of 10^{-4} to 10^{-5} S/cm even when undoped. The question of whether or not doping of well-stacked films will enhance its conductivity to the same extent as doping of bulk material is now being addressed.

5. Conclusion

As presented in the foregoing, the OMBE method has not yet moved beyond the basic research stage. Currently work on organic films made by the OMBE system is mainly concerned with comparison with films made by conventional means. It is the author's intention to pursue organic molecular beam research so that this method will lead to an organic molecular beam epitaxy method. It is the author's hope that the OMBE method will provide a powerful means of creating functional films toward the goal of creating "molecular devices," and that the method will grow beyond the technique of film formation and attain the rank of a scientific field in its own right.

References

1. For example, see "Molecular Beam Epitaxy Technology," (Kiyoshi Takahashi, editor), Industrial Research Association, 1983.
2. Industrial Materials, Nikkan Kogyo Shimbun, Inc., 31, November 1983, p 33.
3. Natsu Ueda, "Thin Film Handbook," Ohm Corp., 1983, p 384.
4. H. Inokuchi, et al., BULL. CHEM. SOC. JPN., Vol 34, 1961, p 749.
5. (a) J.L. Gland and G.A. Somorjai, SURFACE SCI., Vol 38, 1973, p 157.
(b) L.E. Firment and G.A. Somorjai, Ibid., Vol 55, 1976, p 413.
(c) L.L. Atanasoska, J.C. Bucholz, and G.A. Somorjai, Ibid., Vol 72, 1978, p 189.
(d) L.E. Firment and G.A. Somorjai, Ibid., Vol 84, 1979, p 275.
(e) J.C. Bucholz and G.A. Somorjai, J. CHEM. PHYS., Vol 66, 1977, p 573.

6. (a) N. Uyeda, M. Ashida, and E. Suito, J. APPL. PHS., Vol 36, 1965, p 1453.
(b) M. Ashida, BULL. CHEM. SOC. JPN., Vol 39, 1966, p 2625.
(c) N. Uyeda, et al., J. CRYST. GROWTH, Vol 26, 1974, p 267.
7. Yase, Inaoka, and Okada, SOLID STATE PHYSICS, Vol 21, 1986, p 301.
8. "Electronics," Ohm Corp., Vol 32, February 1987, p 3.
9. H. Sasabe, et al., Proc. International Symposium of Molecular Electronic Devices, in press.

20138/9365

Ultrathin Monocrystals Using Van Der Waals Epitaxy

43063801g Wako-shi BUNSHISEI CHOHAUMAKU in Japanese Jan 88 pp 55-62

[Article by Atsushi Koma, Faculty of Science, Tokyo University]

[Text] 1. Introduction

Heterostructure substances in which monocrystalline ultrathin films of two or more substances are stacked together are man-made substances not found anywhere in nature, and they are opening new possibilities in technology. By recently developed molecular beam epitaxy (MBE) and metalloorganic chemical vapor deposition (MOCVD) methods, superlattices in which are stacked alternating single-atom layers, combinations of GaAs and AlAs, have actually been prepared.¹ Ultrathin heterostructures in which the thickness is controlled at the atomic layer level have brought superlattice elements and quantum well semiconductor lasers into the realm of reality, and have provided clues to the discovery of new phenomena, such as the fractional quantum hole effect, which are of considerable interest from a purely scientific standpoint. The successful preparation of ultrathin monocrystals and ultrathin heterostructures is having a considerable impact on both pure science and applications; at the present stage, however, the fabrication of good-quality monocrystalline ultrathin films can be achieved only with extremely restricted combinations of semiconductors, such as GaAs-AlAs having an exceedingly low rate of lattice mismatch, on the order of 0.1 percent. The reason for such limited success lies in the existence of dangling bonds on the cleaned surface of ordinary substances, which means that good-quality ultrathin heteros cannot be grown without satisfying stringent lattice matching conditions.

Focusing on the fact that hetero growth on layered substances free of dangling bonds on the surfaces proceeds only by mediation of the Van der Waals force, so that sufficiently high-quality ultrathin monocrystals can be grown heterogeneously without satisfying the lattice matching conditions, we have demonstrated the feasibility of such a growth process and named it Van der Waals epitaxy.²⁻⁴ This accomplishment has paved the path for the fabrication of ultrathin monocrystals by combining a variety of layered substances outside of the restrictions regarding lattice matching conditions. In the following, we shall discuss the underlying principles of the Van der Waals epitaxy method, and describe the results of applying the method to a tellurium-selenium system, the simplest system to

which the method can be applied. This will be followed by a discussion of the preparation and evaluation of ultrathin monocrystals using a transition metal dichalcogenite substance.

2. Principles of the Van der Waals Epitaxy Method

As a general rule, on a solid surface the termination of the regular array of atoms at the surface results in ruptured bonds, giving rise to dangling bonds, as shown in Figure 1(a). Consequently, when an attempt is made to cause substance A to grow on the monocrystal surface of substance B when the substances have different crystal structures or lattice constants, not all dangling bonds can be connected; this results in a polycrystalline structure of the upper substance or a monocrystalline structure containing large numbers of distortions and defects, resulting in poor-quality crystalline formation. Therefore, a prerequisite to the formation of a good-quality heterostructure is that the substances used to comprise the heterostructure have compatible lattice constants. This, however, imposes a considerable restriction on the types of substances that can be combined to form heterostructures. However, in certain situations conceivably it should be possible to achieve hetero growth by combining substances freely without regard to the lattice matching restriction. Specifically, on a surface free of dangling bonds, such as the cleaved surface of tellurium or selenium or the cleaved surface of layered substances such as $2H-MoS_2$, it should be possible to induce hetero growth of the same substance. In such a case, since no dangling bonds exist on the growth surface, it should be possible to produce good-quality hetero growth film structures even when the lattice matching conditions are not satisfied. Since in such cases the hetero growth proceeds only through the mediation of the Van der Waals force, such hetero growth is called Van der Waals epitaxy. Since the Van der Waals epitaxy method produces hetero growth on a surface free of dangling bonds, it can realize a sharply defined hetero surface relatively free of defects. As such, the method is expected to play an important role in the fabrication of ultrathin monocrystals.

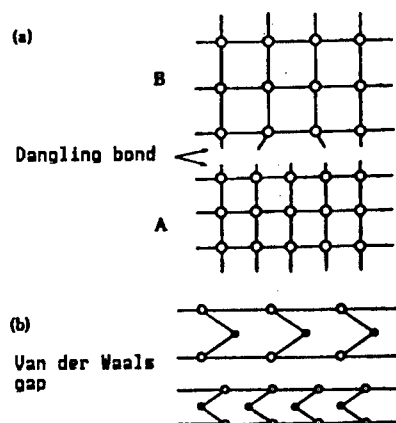


Figure 1. (a) Ordinary Hetero Surfaces, and
(b) Hetero Surfaces Separated by a Van der Waals Gap

3. Van der Waals Epitaxy Apparatus

The type of molecular beam epitaxy apparatus shown in Figure 2 was used to fabricate Van der Waals epitaxy ultrathin films. Because of the high vapor pressure of selenium, an oil diffusion pump equipped with a liquid nitrogen trap (model CCT-150 made by the British VG Corp. was used as the main exhaust pump, in place of an ion pump that is an inherently closed system. When baked at 200°C, the pump can easily attain a 5×10^{-9} Pa vacuum; however, when a selenium raw material is set in the apparatus, no baking can be carried out due to vapor pressure considerations. Although the experiments described below were conducted without baking, by using the above mentioned main exhaust pump, a titanium sublimation pump, and a liquid nitrogen shroud, an ultrahigh vacuum of 3×10^{-8} Pa was attained without baking. A Knudsen cell was used as the selenium source. For the supply of niobium, molybdenum, and other high-melting point metals, an electron beam vaporization source (model EG2Mk-II made by VG Corp.) was used. Since this electron beam vaporization source was an electrostatic bias type, rather than the more widely used magnetic bias type, it entailed no danger of producing a leak magnetic field, which would have affected the electron energy analyzer installed for evaluation purposes; thus, the particular vaporization source was well suited to our purposes. The equipment was capable of raising the substrate temperature up to 900°C through the use of a resistor heater. A quartz oscillator film thickness meter placed next to the substrate provided a means of measuring the thickness of the films grown.

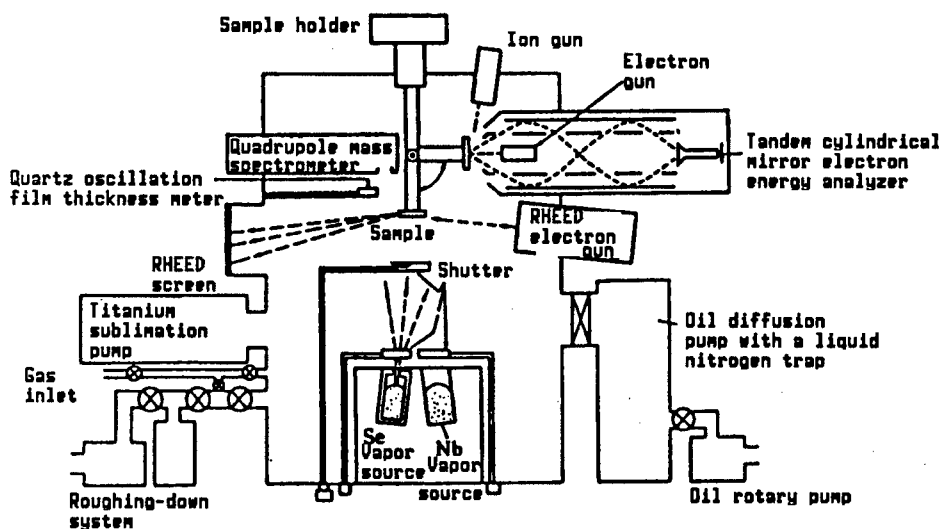


Figure 2. Schematic Diagram of Monolayer Film Monocrystal Preparation and Evaluation Equipment

Since ultrathin monocrystalline films less than 1 nm thick are subject to deterioration when exposed to air, as far as possible any samples produced should be evaluated in situ. For this purpose, the apparatus contained the

following types of electron spectroscopy equipment: a reflection high-speed electron beam diffraction (RHEED) device, which was used to monitor the crystallinity and lattice intervals of the film being grown on a real-time basis; a grown sample was subjected to a tandem cylindrical mirror energy analyzer with a built-in electron gun (model 15-2255 G, made by the U.S. PHI Corp., its composition was tested using the Auger electron spectra, and its electron structure was determined from low-speed electron energy loss spectra (LEELS).

In LEELS, low-speed electrons, about 100 eV, are allowed to strike the sample, inducing electron transition and plasmon excitation near the sample surface. Then, data on the electron structure of the sample are obtained by measuring the energy distribution of electrons which return to the sample after losing some of their energy.⁵ By varying the energy level of incident electrons from 10 eV to 2000 eV, the technique allows variation in the probing depth from approximately 0.2 nm to 1.1 nm.⁶ For this reason, LEELS is especially well suited to the evaluation of the ultrathin film monocrystals measuring 1 nm or less fabricated in this work.

4. Hetero Growth of Selenium Ultrathin Film Monocrystals on a Tellurium Cleaved Surface

Elemental semiconductor materials belonging to Group VI in the periodic table, tellurium and selenium have a peculiar crystal structure consisting of hexagonally aligned helixes, as shown in Figure 3. Although the atoms within a helix are joined by strong covalent bonds, the atoms belonging to different helixes are joined only by the weak Van der Waals force. Consequently, a crystal can easily be cleaved along helixes, so that no dangling bonds appear on the cleaved surface. Thus, cleaved crystals can be used to advantage in Van der Waals epitaxy. To test the usefulness of Van der Waals epitaxy, we tried to grow a selenium ultrathin film on a tellurium monocrystal cleaved surface having a lattice constant differing from the lattice constant of selenium by as much as 20 percent. After cleaving its monocrystal sample, the tellurium substrate was placed in the molecular beam epitaxy device as shown in Figure 2, and was cleaned under a 3×10^{-8} Pa ultravacuum by heating it to 200°C. Hetero growth was conducted at a rate of 0.01 - 0.1 nm/s by maintaining the substrate temperature at 80°C. The thickness of the films grown was monitored using a quartz oscillation film thickness meter. The monocrystallinity of the prepared ultrathin films was checked by the RHEED device using an acceleration voltage of 25 kV. Figure 4(a) [not reproduced] shows the RHEED pattern of the tellurium substrate. The lattice intervals observed agreed well with published data. No surface rearrangement was observed.

Figure 4(b) [not reproduced] shows the RHEED pattern measured after a selenium ultrathin film 0.4 nm thick was grown. The photograph clearly shows a streak pattern in which the lattice intervals of selenium crystals are aligned accurately with the streak pattern of substrate tellurium crystals. As shown in Figure 4(c) [not reproduced], the RHEED pattern of selenium emerges even more clearly when measurements are taken after selenium monocrystals 600 nm thick are grown. Since Figures 4(a) through 4(c) are on the same scale, from these illustrations it can be seen clearly

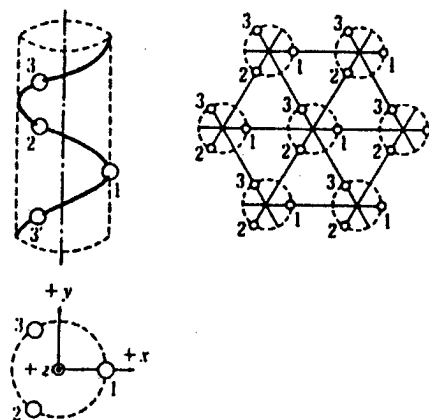


Figure 3. Crystal Structures of Selenium and Tellurium

that selenium monocrystals, even though differing from the lattice intervals of the substrate tellurium crystals by 20 percent, started growing from the very first layer on the substrate surface according to their own lattice intervals. This fact, a significant advantage of Van der Waals epitaxy, is in sharp contrast to the situation prevailing in the distorted superlattice⁷ in which the lattice intervals of the ultrathin film to be hetero grown are forced to match those of the substrate crystals. Furthermore, whereas a distorted superlattice cannot achieve good-quality hetero growth if the unit ultrathin film thickness is larger than a few nm, Van der Waals epitaxy knows no such restrictions and can produce films having a high degree of monocrystallinity.

The results of Auger electron spectroscopy and low-speed electron energy loss spectroscopy conducted in addition to the RHEED observations show a close resemblance between the spectra of the prepared selenium ultrathin film--despite the fact that it is only 0.4 nm thick--and the spectra of bulk selenium monocrystals, indicating that Van der Waals epitaxy is capable of producing sufficiently good quality ultrathin film monocrystals.

5. Van der Waals Epitaxy of Transition Metal Dichalcogenite Substances

There is a group of transition metal dichalcogenite substances well suited to Van der Waals epitaxy. As shown in Figure 5, these substances have a layered crystal structure wherein a layer consisting of transition metal atoms, held between chalcogen atoms, constitutes the unit layer. Although the atoms within a unit layer are strongly bonded, between layers atoms are weakly bonded only by the Van der Waals force. For this reason, such a substance can easily be cleaved along layers, and the cleaved surface is free of dangling bonds,⁸ offering a site for Van der Waals epitaxy. Transition metal dichalcogenites include semiconductors such as MoS_2 , insulators such as HfSe_2 , and even metal superconductors such as NbSe_2 . By suitable combination of these substances, it was thought, it should be possible to create a variety of ultrathin film hetero structures not achievable with other methods. The following discusses the Van der Waals epitaxy of transition metal dichalcogenites, with particular focus on the ultrathin film hetero growth⁹ of NbSe_2 on the cleaved surface of a semiconductor 2H-MoS_2 .

NbSe₂ was hetero grown on a clean cleaved surface of a naturally occurring molybdenite crystal by using the equipment shown in Figure 2. Growth was attained with a substrate temperature of 700°C and a growth rate of approximately 0.01 nm. Figures 6(a) and 6(b) show, respectively, RHEED patterns of the 2H-MoS₂ substrate and of an NbSe₂ ultrathin film (unit layer) 0.6 nm thick grown on that substrate. As with the case of the selenium ultrathin film on tellurium, the photographs show clearly that high-quality NbSe₂ monolayer film monocrystals, while maintaining their own lattice intervals, grew on a MoS₂ cleaved surface differing in lattice intervals by 9 percent. Although in this case the hetero grown film and the substrate have different lattice intervals, it has been confirmed that the directions of their a-axes are in perfect agreement.

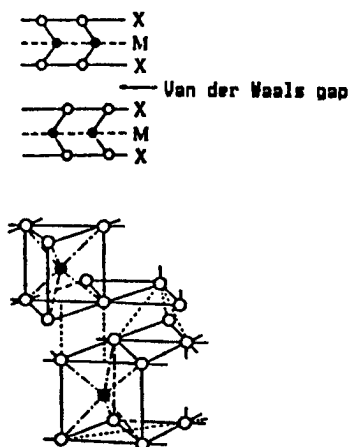


Figure 5. Crystal Structure of Transition Metal Dichalcogenites

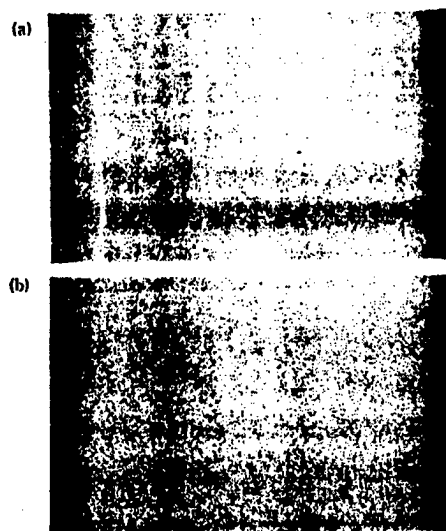


Figure 6. (a) RHEED Patterns of 2H-MoS₂ Substrate
(b) RHEED Patterns of NbSe₂ Monolayer Film
0.6 nm Thick Hetero Grown on the Above
Substrate

Figure 7 shows Auger spectra of 2H-MoS₂ substrate, NbSe₂ ultrathin film 0.6 nm thick hetero grown on the substrate, and the cleaved surface of NbSe₂ monocrystals. Although, due to the thinness of the film, signals from the film are overlapped with signals from the MoS₂ substrate, the Auger spectra of the NbSe₂ ultrathin film are very similar to those of NbSe₂ monocrystals, and it is clear that the composition of the prepared ultrathin films was not something that was intentionally controlled.

Figure 8 shows LEELS spectra of the valence electron excitation regions of the above-mentioned MoS₂ substrate, NbSe₂ ultrathin film, and the NbSe₂ monocrystal cleaved surface. These spectra were measured by using an

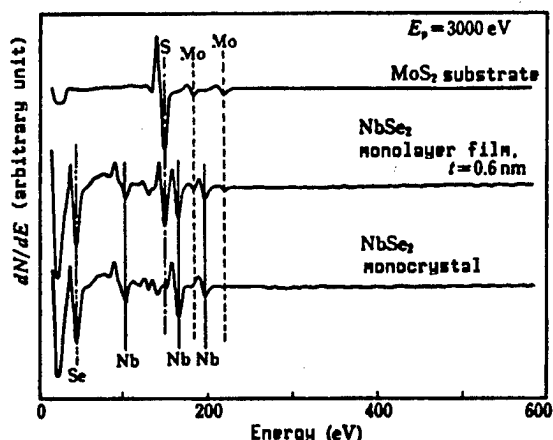


Figure 7. Auger Spectra of: 2H-MoS₂ Substrate, NbSe₂ Monolayer Film 0.6 nm Thick Hetero Grown on That Substrate, and Cleaved surface of 2H-NbSe₂ Monocrystals

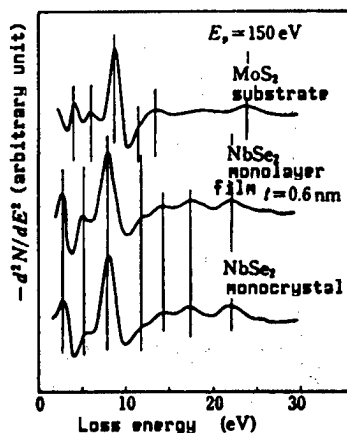


Figure 8. LEELS Spectra of: 2H-MoS₂ Substrate, NbSe₂ Monolayer Film 0.6 nm Thick Hetero Grown on That Substrate, and Cleaved Surface of 2H-NbSe₂ Monocrystals

incident electron energy of 150 eV. Since the depth of probing was around 0.3 nm, less than that used in Auger electron spectrometry, this probing depth would have been able to measure spectra on an ultrathin film only 0.6 nm thin without interference from the substrate. In fact, as indicated by the illustration, the LEELS spectra of the NbSe₂ ultrathin film are in perfect agreement with those of the NbSe₂ monocrystal cleaved surface. This would seem to suggest strongly that Van der Waals epitaxy is capable of producing high-quality, ideal ultrathin film monocrystals without causing island-like hetero film growth or mixed crystals through mutual diffusion.

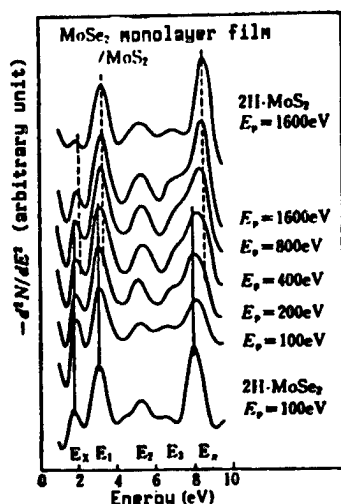


Figure 9. Auger Spectra Determined at Various Locations in a 5 mm x 5 mm Area of an NbSe₂ Monolayer Film Hetero Grown on 2H-MoS₂ Substrate (measured at 4 vertices and center)

Figure 9 shows Auger spectra of measurements taken at various locations within a 5 mm x 5 mm area of the sample surface in order to assess the uniformity of NbSe₂ film thickness. As the illustration shows, the ratio of the Auger signals from the NbSe₂ ultrathin film to the Auger signals from the MoS₂ substrate, observed through the ultrathin film, is constant irrespective of the location of measurement, indicating that the grown film has a uniform thickness of 0.65 ± 0.05 nm.

In addition to growing NbSe₂ ultrathin film monocrystals on MoS₂ we also successfully prepared MoSe₂ ultrathin film monocrystals on a cleaved surface of 2H-MoS₂. On the samples thus obtained, we measured the probing depth from 0.2 nm to 1 nm by varying the incident electron energy between 100 eV and 1600 eV. Figure 10 shows the resulting LEELS spectra. For comparison purposes, the LEELS spectra of a 2H-MoS₂ monocrystal cleaved surface and those of 2H-MoS₂ are also presented. In the illustration, Ex denotes a loss peak due to electron excitation, E₁-E₃ denote loss peaks due

to electron transition from the valence band to the conduction band, and $E\pi$ denotes a loss peak due to partial plasmon excitation. The peaks in the LEELS spectra of the MoSe_2 ultrathin film, at an incident electron energy level of 400 eV or less, show a fair degree of agreement with the peaks of MoSe_2 monocrystals, and above 400 eV they agree fairly well with those of MoS_2 in the substrate. This suggests strongly the existence of a sharp surface terrain in the neighborhood of 0.6 nm, which is the probing depth employed with an incident electron energy level of 400 eV. This demonstrates that Van der Waals epitaxy is capable of creating sharply defined ultrathin film hetero surfaces.

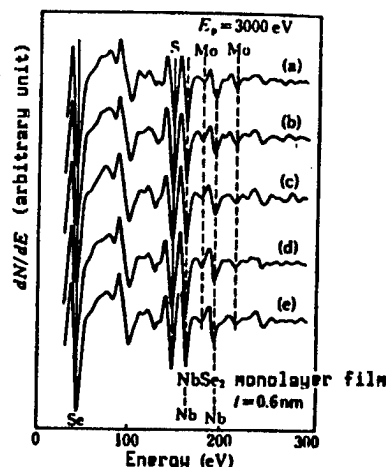


Figure 10. Nondestructive Depth Direction Analysis by LEELS of NbSe_2 Monolayer Film 0.6 nm Thick Hetero Grown on 2H- MoS_2 Substrate

In addition to the above combinations, we also confirmed successful growth of NbSe_2 monolayer film monocrystals on MoSe_2 . These results indicate that through use of the Van der Waals epitaxy method, any combination of transition metal dichalcogenite substances can be utilized for creating ultrathin film monocrystals.

6. Conclusion

We developed a new method of Van der Waals epitaxy, and using this method successfully created high-quality ultrathin film monocrystals measuring less than 1 nm thick. This method has opened the possibility of creating ultrathin film monocrystals by almost any combination of a variety of transition metal dichalcogenites, including superconducting metals, semiconductors, and insulators.

The ultrathin film metal-semiconductor structures created in the present investigation seem to be especially well suited to the realization of high-temperature superconductors based on the exciton mechanism and proposed by Allender, Bray, and Bardeen.¹⁰ To realize this goal, it is necessary to form a metal ultrathin film about 1 nm thick on a semiconductor; however, thus far this goal has eluded our grasp due to lack of an adequate means of

creating metal ultrathin films of a high degree of perfection. Since the Van der Waals epitaxy method allows the hetero growth of high-quality metal NbSe₂ ultrathin films on the MoS₂ semiconductor, it will be possible to actually implement the structure proposed by Allender, et al. Currently measurements are being taken on the superconducting properties of ultrathin film metal-semiconductor structures prepared in this manner.

Since the ultrathin film monocrystals made by the Van der Waals epitaxy method have a high degree of semiconductor perfection, as described above, the method should find wide applications beyond the field of exciton superconductivity. It is hoped that the work presented herein will help to open new application areas for Van der Waals epitaxy.

References

1. P.M. Petroff, A.C. Gossard, W. Wiegmann, and A. Saage, J. CRYSTAL GROWTH, Vol 44, 1978, p 5.
2. A. Koma, K. Sunouchi, and T. Miyajima, MICROELECTRONIC ENGNG., Vol 2, 1984, p 129.
3. Ibid., J.V AC. SCI. TECHNOL., Vol B3, 1985 p 724.
4. A. Koma, Extended Abstracts 17th Conf. Solid State Devices and Mater., Tokyo, 1985, p 13.
5. Atsushi Koma, Katsumichi Yagi, Katsu Tsukada, and Kazumasa Aono (authors and editors), "Surface Physics Engineering Handbook," Maruzen, 1987, p 205.
6. K. Yoshimura and A. Koma, Extended Abstracts 16th (1984 Intern.) Conf. Solid State Devices and Mater., Kobe, 1984, p 293.
7. G.C. Osbourn, J. APPL. PHYS., Vol 53, 1982, p 1586.
8. A. Koma and K. Enari, Proc. Intern. Conf. Phys. Semicon., Edinburgh, 1978 (Inst. Phys. Conf. Ser.) No 43, 1979, p 895.
9. A. Koma, K. Sunouchi, and T. Miyajima, Proc. Intern. Conf. Phys. Semiconduc., San Francisco, 1984 (Springer-Verlag, New York, 1985), p 1465.
10. D. Allender, J. Bray, and J. Bardeen, PHYS. REV., Vol B7, 1973, p 1020.
11. A. Koma and K. Yoshimura, SURFACE SCI., Vol 174, 1986, p 556.

20138/9365

- END -

10

This is a U.S. Government publication. Its contents in no way represent the policies, views, or attitudes of the U.S. Government. Users of this publication may cite FBIS or JPRS provided they do so in a manner clearly identifying them as the secondary source.

Foreign Broadcast Information Service (FBIS) and Joint Publications Research Service (JPRS) publications contain political, economic, military, and sociological news, commentary, and other information, as well as scientific and technical data and reports. All information has been obtained from foreign radio and television broadcasts, news agency transmissions, newspapers, books, and periodicals. Items generally are processed from the first or best available source; it should not be inferred that they have been disseminated only in the medium, in the language, or to the area indicated. Items from foreign language sources are translated. Those from English-language sources are transcribed, with the original phrasing and other characteristics retained.

Headlines, editorial reports, and material enclosed in brackets [] are supplied by FBIS/JPRS. Processing indicators such as [Text] or [Excerpts] in the first line of each item indicate how the information was processed from the original. Unfamiliar names which are rendered phonetically or transliterated by FBIS/JPRS are enclosed in parentheses. Words or names preceded by a question mark and enclosed in parentheses were not clear from the original source but have been supplied as appropriate to the context. Other unattributed parenthetical notes within the body of an item originate with the source. Times within items are as given by the source.

SUBSCRIPTION/PROCUREMENT INFORMATION

The FBIS DAILY REPORT contains current news and information and is published Monday through Friday in 8 volumes: China, East Europe, Soviet Union, East Asia, Near East & South Asia, Africa (Sub-Sahara), Latin America, and West Europe. Supplements to the DAILY REPORTs may also be available periodically and will be distributed to regular DAILY REPORT subscribers. JPRS publications generally contain less time-sensitive information and are published periodically. Current JPRS publications are listed in *Government Reports Announcements* issued semi-monthly by the National Technical Information Service (NTIS), 5285 Port Royal Road, Springfield, Virginia 22161 and the *Monthly Catalog of U.S. Government Publications* issued by the Superintendent of Documents, U.S. Government Printing Office, Washington, D.C. 20402.

U.S. Government offices may obtain subscriptions to the DAILY REPORTs or JPRS publications (hardcovers or microfiche) at no charge through their sponsoring organizations. DOD consumers are required to submit requests through appropriate

command validation channels to DIA, RTS-2C, Washington, D.C. 20301. (Telephone: (202) 373-3771, Autovon: 243-3771.) For additional information or assistance, call FBIS, (703) 527-2368, or write to P.O. Box 2604, Washington, D.C. 20013.

The public may subscribe to either hardcover or microfiche versions of the DAILY REPORTs and JPRS publications through NTIS at the above address or by calling (703) 487-4630. Subscription rates will be provided by NTIS upon request. Subscriptions are available outside the United States from NTIS or appointed foreign dealers. Back issues or single copies of the DAILY REPORTs and JPRS publications are not available. New subscribers should expect a 30-day delay in receipt of the first issue.

Both the DAILY REPORTs and the JPRS publications are on file for public reference at the Library of Congress and at many Federal Depository Libraries. Reference copies may also be seen at many public and university libraries throughout the United States.